UNIVERSITY OF OKLAHOMA

GRADUATE COLLEGE

BEAD WIDTH AND HEIGHT EFFECTS ON POLYMER ADDITIVE MANUFACTURING MATERIAL PROPERTIES

A THESIS

SUBMITTED TO THE GRADUATE FACULTY

In partial fulfillment of the requirements for the

Degree of

MASTER OF SCIENCE

By

RYAN BERNARDY

Norman, Oklahoma

2025

BEAD WIDTH AND HEIGHT EFFECTS ON POLYMER ADDITIVE MANUFACTURING MATERIAL PROPERTIES

A THESIS APPROVED FOR THE

SCHOOL OF AEROSPACE AND MECHANICAL ENGINEERING

BY THE COMMITTEE CONSISTING OF

Dr. Yingtao Liu, Chair

Dr. Chris Billings

Dr. Jivtesh Garg

Acknowledgements

I first would like to thank my wife Kaylee Bernardy for the support during my degree and the joy she brings to my life. All of the late nights working on homework or processing data were enabled or otherwise made easier by her support and I cannot thank her enough.

I would next like to thank Dr. Yingtao Liu for his support throughout my time at OU and his dedication to his students. In the last two years I have benefitted greatly in learning from his guidance working through the process of publication and graduate level academia.

I would also like to thank Dr. Chris Billings for his expertise and assistance with data acquisition in addition to agreeing to co-chair my thesis committee. I also thank my colleagues and peers Rudy Villa and Joshua Hall for sharing their knowledge in materials testing which helped progress my testing schedule. Also thank you to Dr. Garg for generously lending me your time and expertise as part of my thesis committee.

Thank you to everybody involved in my leadership at Tinker throughout both the application and completion of this degree and it's funding. Jason Mann, Kyle Taylor, Ryan Fowler, Jason McCurry, Glen Drebes, Jordan Johnston, Julie Hines, Eamon Needler, thank you all for helping provide me with this opportunity to excel. I also thank my coworkers who have been supportive throughout application and completion of this degree and helped with the start and stop of work during this. Alexander Zoefrea, Daniel Shelton, Todd Bayles, Trent Pence, Jeremy Tate, Al Andrade, Alexander De Jesus, and Colton Bohannon.

Thank you to my peers I have spent many hours studying with; Jordan Tupper, Kevin Pham, Alfredo Hernandez, Zach Bennett, Richard Banks, Forrest Raines, Emanuel De Leon, and Octavio Mejia.

Last but not least I would also like to thank the SMART program for the opportunity to further my education while performing research for my employer and acknowledge this research as funded by OUSD/R&E (The Under Secretary of Defense-Research and Engineering), National Defense Education Program (NDEP)/BA-1, Basic Research Via SMART Scholarship.

Table of Contents

Table of Figures

Table of Tables

Abstract

Ultem 9085 resin is used notably in aerospace applications due to a combination of its high performance mechanically and thermally for a thermoplastic, processability as a thermoplastic, and achieving flame smoke toxicity (FST) ratings. Additive manufacturing (AM) has become a prominent manufacturing method for this material in aerospace use as it has achieved certifications for airworthiness which substantiates it's use on planes. Differences in mechanical properties between different bead widths and heights have been noted however a more complete analysis of bead width and height with changing mechanical properties is needed for FDM printed thermoplastics for the link between these properties to be explored. The present work aims to establish a dataset of these values, made specifically with a material of interest for use, so that the link between these values and mechanical properties can be investigated. In this thesis XY, YX and +/- 45deg samples of Ultem 9085 were fabricated with varying bead widths and heights utilized during printing across two nozzle size selections which were then tensile tested per ASTM D638 standard to create a dataset for analyzation. This dataset was then analyzed to look for trends for exploring the link between the two. During this process direct image correlation (DIC) was taken with a portion of samples in addition to scanning electron microscopy imaging of breakages for any potential insights these could provide to the data, batches of samples that were noted to have a flaw within any of the batch were retained and tested for any insights that could be gathered in future works regarding printing defects.

Chapter 1: Introduction

1.1 Uses, Certification, and FDM Manufacturing of Ultem 9085

Fused Deposition Modeling (FDM) manufacturing has seen a growing use in the last several decades, for aerospace use direct part or component manufacture in addition to tooling for repair or manufacture of aircraft or their respective parts is applicable. This manufacturing method as a minimal tooling method where design complexity has minimal manufacturing costs allows significant upsides for one-off or short manufacturing runs when comparing to traditional manufacturing methods.

Ultem 9085 has high mechanical, chemical resistance, and thermal performance for a thermoplastic. These properties coupled with its FST properties has led to certification [1] of mechanical properties when manufactured under constrained sets of FDM manufacturing parameters, adding this to materials traceability and the material becomes airworthy. These certifications exist specifically for interior parts that structurally are non-critical for this material on Stratasys machines utilizing their proprietary environment consisting of; machine, software, material, and process. This is a highly advantageous thing to have in the aerospace industry however the constraints for processing can leave some designs wanting for parameters outside of the parameters accessible within the “locked down” environment for certifications. Differing mechanical specifications for differing bead widths and heights [2] does tell us that there is a reason for the process being locked down, changing these parameters too much will change the material properties. Even if some certifications would still require empirical testing it would be advantageous for engineers in the industry to have tools for estimating the effects of these parameter changes to use where they can.

Ultem 9085 can be manufactured through FDM methods the same as other thermoplastics, however it is a difficult material to print due to it's high processing temperatures. This means Ultem 9085 typically requires a heated enclosure for process control to prevent warpage. This generally leaves Stratasys, which until it's recent expiration held the patent for a heated enclosure with external motors [3], as the primary method of FDM manufacture for this material. In this thesis the Essentium HSE 180 system was used with both Essentium and Stratasys Ultem 9085 filament due to the ability to select a wider range of bead widths and heights in printing settings than the Stratasys options.

1.2 State of the Art for Polymer Additive Manufacturing

FDM printing is generally described by extruding stock filament material through a heating nozzle onto a build surface to layer by layer deposit a bead of polymer material in a programmed pattern until the print finishes producing a model for post-processing into an end product. Similar to milling, a traditional manufacturing method, this is performed with computer numerical control (CNC) machines but with an FDM toolhead for depositing materials (displayed in Figure 1.) from a stock material supply instead of a spindle for removing material from a stock shape of material. The "slicer" is what the computer-aided manufacturing (CAM) software is typically called which is utilized for these machines to turn digital models into processable machine code.

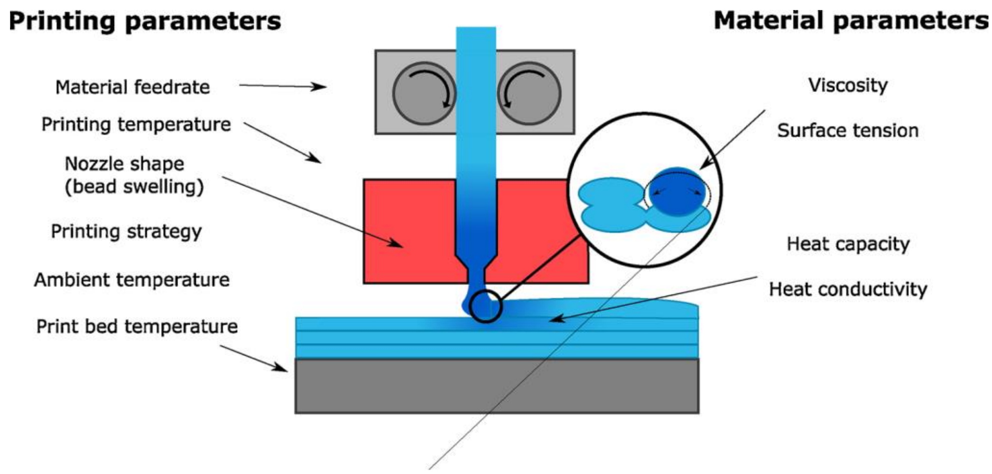

Figure 1: Diagram displaying FDM printing technique and associated variables. [4]

FDM printing has other material advances which are also state of the art advances even if they are not the topic of this thesis. Most notably composite materials manufactured with FDM technologies are part of the latest advances with manufactures having produced and sold industrial additive manufacturing production equipment utilizing continuous and discontinuous fiber reinforcement [5-8]. The state of the art also includes advances such as additional machine axes [9], subtractive capabilities [5, 8], pellet feed [5, 8, 9], and annealing procedures [10].

There are other notable additive manufacturing methods which are not focused on within the scope of this thesis as this thesis focuses on FDM printing. For polymers the notable additions would be selective laser sintering (SLS), laminated object manufacturing (LOM), automated tape placement (ATP), and photopolymer resin printing techniques; stereolithography (SLA), direct light projection (DLP), direct ink writing (DIW). There are additionally many different thermoplastic polymers which are used for FDM manufacturing besides Ultem 9085 however these materials were not analyzed in this thesis as this would quickly compound the testing requirements while in theory being unnecessary to establish the concepts and relationships between the manufacturing parameters and the resulting effects on material properties. The author would like to note that choosing an amorphous polymer for the test material also has the benefit of avoiding the possibility of crystallinity effects which simplifies analyzation for the initial works investigating these effects albeit at the drawback of not capturing the effects of crystallinity effects within the dataset made.

1.3 Previous Work, Characterizations of Ultem 9085 FDM Properties

Previous work has been performed on characterizing Ultem 9085 due to these motivating interests mentioned in the preceding subsections. There has been work on the effect of printing direction [11, 12], characterization of various mechanical and thermal properties [13-16], post-processing impacts [17], and FST properties [18]. The researchers involved have included both academic and private industry researchers investigating properties, and thus, this thesis references both as appropriate.

Printing orientation was analyzed by Kuzmina et, al. [11] for the effect on Ultem 9085 bending properties in conjunction with cooling conditions. This study involved printing ASTM D790-17 flexural samples of Ultem 9085 of differing infill patterns which were allowed to cool under differing conditions then tested for both static and fatigue bending tests. The testing did not uncover significant effects on mechanical properties under differing cooling conditions although it did note that the surface finish was better in the samples cooled slower.

Printing orientation was also analyzed by Zaldivar et al. [12], with the thermal and mechanical properties investigated. The infill patterns are described as the sample "macrostructure," with analysis performed noting the extrusion bead similarities in behavior to fiber tows in laminated composites, describing them as "polymeric fibers" and comparing mechanical results to the volume fraction of aligned polymeric fibers. A major conclusion of this study in addition to the mechanical results was the additively manufactured samples behavior similarities to composite structures.

Zaldivar et, al. [15] in a separate publication analyzed filament moisture content and the effect it has on the mechanical properties of additively manufactured Ultem 9085. In this study, filament was exposed to moisture, and a model was developed for obtaining diffusion coefficients for determining acceptable limits before material would be contaminated with an unacceptable moisture content and the timeframes required to dry material. The samples were tested with limits of 0.16% moisture content found as the point where porosity is found due to moisture expansion during heating and mechanical properties significantly suffer. Timeframes were estimated for material stored inside and outside of the manufacture machine before the material would exceed moisture specifications of the manufacturer.

Thermal aging influences on Ultem 9085 mechanical properties were studied by Padovano et, al. [14] with ASTM D790 flexural tests and ASTM D638 tensile tests performed for evaluation. The samples were evaluated for the porosity from different sample orientations, but all had the +-45 degree infill pattern. The statistical analysis performed demonstrated a significant effect of cyclical and shock thermal loading on the flexural strength and elastic moduli of the material.

Yifan LV et, al. [18] investigated the fire retardancy of Ultem 9085 at varying infill densities. The study did find the fire retardancy to be related to the infill density with denser samples performing better but noting that even the worst performing samples comfortably passed the vertical burn test and heat release rate tests per FAR 25.853 (Federal Aviation Regulation) requirements.

Annealing changes in Ultem 9085 geometrical and mechanical properties were investigated by Zhang et al. [17] In this study, the ability to mitigate geometrical change without additional fixturing by retaining the support material utilized by Stratasys machines was investigated, finding that there was still a change in geometrical properties due to material stresses relaxing but that the change in geometry was mitigated. Results from DIC analysis demonstrated a decrease in stress concentrations with an increase in ductility, this was at the downside of small reductions in tensile strength.

Bagsik et al. [13] performed statistical analysis of Ultem 9085 mechanical properties at varying infill angles testing the effect of modifications to the distance between the center of the infill bead and modifications to the perimeter overlap. This study is the closest related to this thesis as these settings very directly impact the bead profile during deposition; however these settings do not actually change the bead width or height; these settings change how squished the bead is during deposition and thus change the density of the print however at the difference of causing the print to be under or over extruded. The study found that making the parts denser did generally improve mechanical properties and that those properties were heavily dependent on the orientation of the part.

Wratkowski et, al. [16] demonstrated repeatability across several models of additive manufacturing machines produced by Stratasys with material samples produced over a timeframe with these machines. This study showed part consistency in both dimensions and mechanical properties across the machines utilized. It also showed varying machine hours on different machine systems to demonstrate the machines were consistent at different levels of wear or use. The study utilized ASA, Ultem 9085, and Nylon 12 and also demonstrated consistency in material properties in batches produced weeks apart.

1.4 Thesis Outline

This thesis is designed to generate a dataset for the material properties when manufacturing thermoplastics with the FDM additive manufacturing method with two of the primary manufacturing parameters, deposition bead width and height, varied so that the effects can be analyzed. This dataset is intended to provide an empirical dataset for analyzing Ultem 9085 due to the interest in this particular material and a foundation for observing these effects for amorphous thermoplastics. Chapter 2 will describe the testing setup utilized which will include sample manufacturing details. Chapter 3 will describe the testing performed and the standards used. Chapter 4 will show the results of this work with an overview of the data and any observations from analysis at this time. Chapter 5 will conclude this project and describe desired future work.

Chapter 2: Testing Setup

2.1 Sample Production

Sample production was performed on an Essentium HSE 180 HT printer with both 0.4mm and 0.8mm nozzles utilizing Simplify3D software for slicing. The bead heights were varied between 0.10mm and 0.55mm. Batches of 6 for each sample parameters were manufactured simultaneously in sequentially printed batches for each set of parameters which were then inspected visually and with a magnifier for observable printing flaws in the surfaces. Material was dried in a vacuum oven per Stratasys spec [19] prior to printing and kept in the machine dryer bay during use until the material was either consumed or re-dried. Batches with flaws noted in any samples were retained and tested to produce data regarding failure in flawed samples for use in future works, the entire batch was reprinted in the case of any observed print flaws until proper prints across an entire set of 6 samples were achieved in the same set.

Samples were recorded, numbered, and weighted for density calculations. Any observed flaws were noted on the sample. Samples had targets for video extensometer adhered until a jig was developed by the author for marking targets onto the samples. The marked targets generally worked well however in some cases the extensometer would have difficulty picking up the marked target due to some samples showing a pattern in the marker resulting from sample surface finish, for these samples adhered targets were applied. A total of 528 samples were recorded including retained flawed samples. Upon availability of a direct image correlation (DIC) setup for the test apparatus becoming available a third of samples from remaining sets were separated and prepared for DIC testing with application of a white spray paint layer to the imaged side followed by speckle-coating with a black spray paint.

2.2 Parameters for FDM 3D printing

Samples were produced for XY, YX, and +/- 45deg infill patterns as is typical for 3D layer infill patterns in use and published FDM material specifications.[2, 20-23] The bead heights were noted to not all perfectly produce the designed sample height when aggregated and the aggregated height was noted measuring with calipers after testing during data processing. A singular perimeter was used for both the YX and +/- 45deg infill patterns, no perimeters were used with the XY orientation samples due to redundancy with the infill pattern and avoiding any remnant fill causing the inclusion of beads deviating from the rest of a samples beads.

Simplify settings included an oven temperature of 200C, nozzle temperature 375C, bed temperature 190, and print speed of 55 mm/s. Extrudate cooling was not used, print overlap and bead spacing were adjusted as needed with varying layer height as under extrusion and over extrusion were observed in samples. Magigoo HT bed adhesive was applied to a spring steel print bed after heating via squirt bottle and a rubber brayer type roller.

2.3 Flaws Common to Polymer Additive Manufacturing

There are a handful of flaws common to FDM printing. Moisture is a significant source of sample flaws[15] and one of the primary flaws visual inspection is used for. Over and under extrusion[13] are common factors to control for[24] as they will influence end item mechanical properties. Surface flaws from misprints are additional flaws that are easy to determine with a visual inspection.

Throughout production with changing parameters there were varying print flaws encountered. These flaws ranged from printer errors to settings requiring further dialing in to combinations of both. Common errors were either over or under extrusion while dialing in print settings for a set of parameters, this was particularly noticeable in corners where there would be many infill-perimeter overlaps and this overlap setting being off could compound any errors due to extrusion multiplier. Some samples would have pinhole or void errors which would be marked at the location of the error so that if these samples failed at the error it could be noted for later scanning electron microscopy (SEM) analysis.

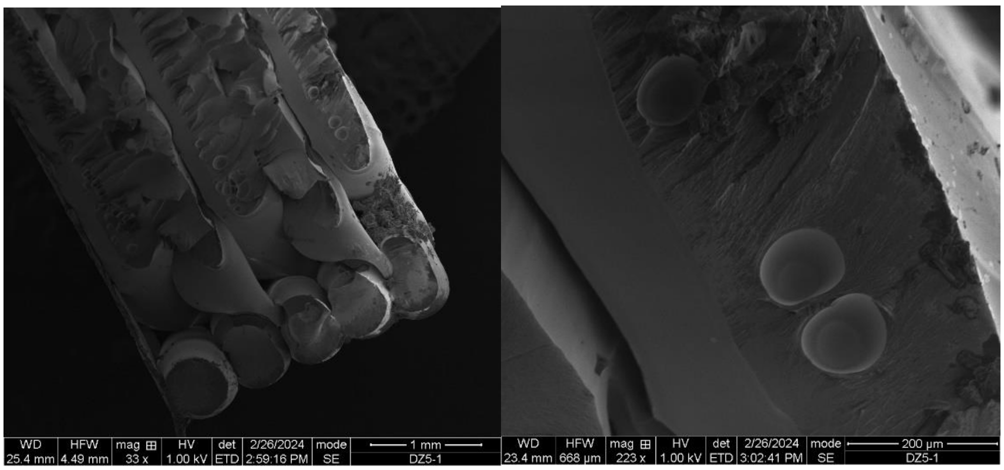

Figure 2: SEM image of sample #40 showing circular flaws from moisture in sample.

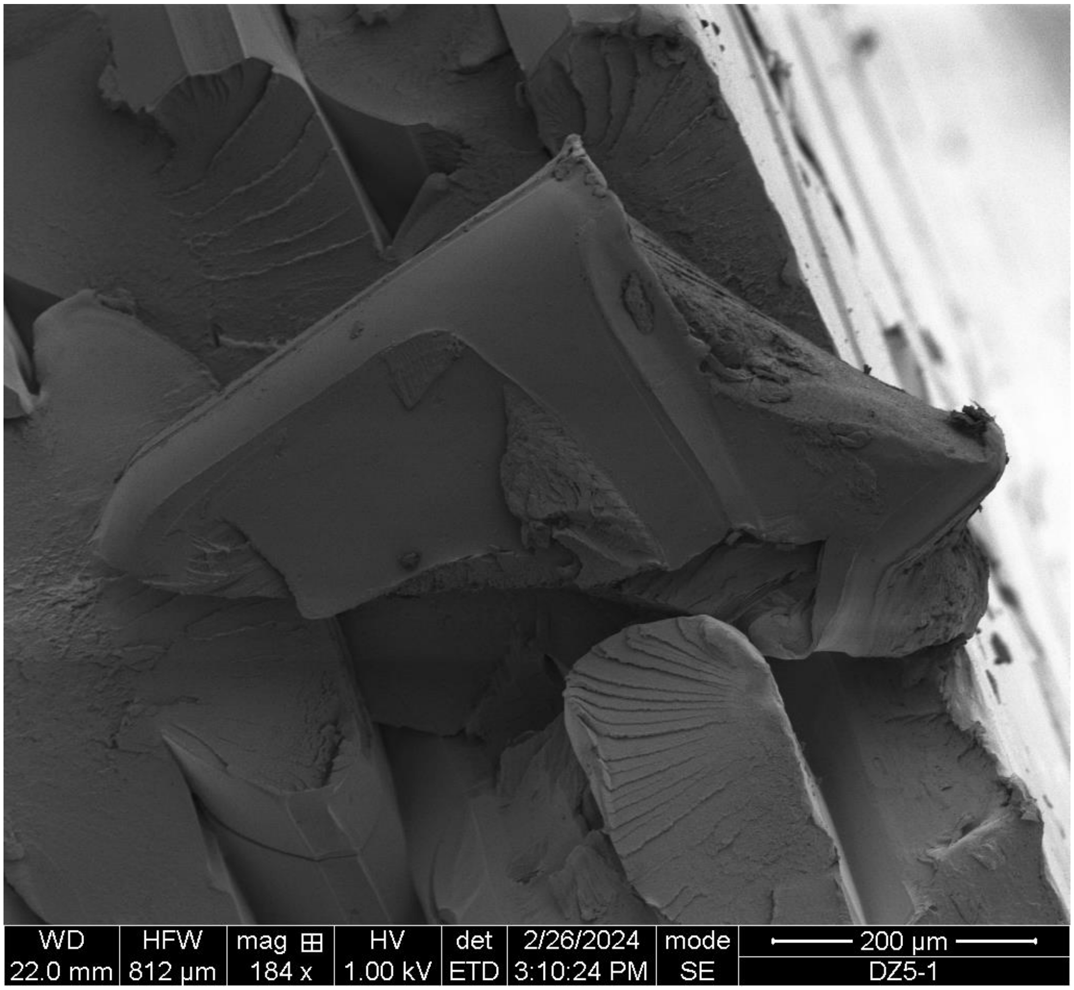

Figure 3: SEM image of surface flaw on sample #40 from unadhered extrudate misprinting as a defect.

Some SEM images were taken of samples at the breakages and at noted flaw locations. The above images are examples of some but not all of the flaws experienced in sample production. SEM images produced in this study were taken from sections of the samples that had been cut off from the primary section with a bandsaw to fit the SEM machine with Au sputter-coating in the sections desired for imaging and attaching the samples to the mounts for imaging using carbon tape and imaged with low (1-10kV) voltage. There were some samples that became contaminated with dirt in the process of testing, bandsawing, and transporting between these processing locations and the SEM room. It was noted that fracturing and tearing of the print beads and surfaces can be observed through this method although the scope of this study did not have capitalizations on this capability, examples are listed below.

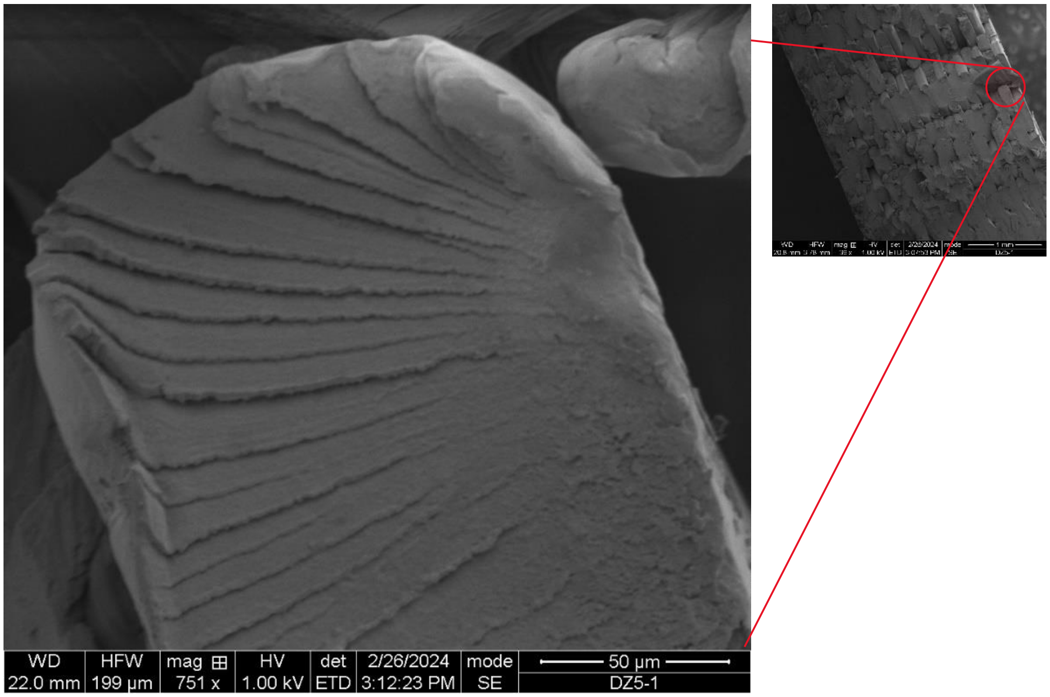

Figure 4: SEM image of stepped fracturing in a toolpath bead.

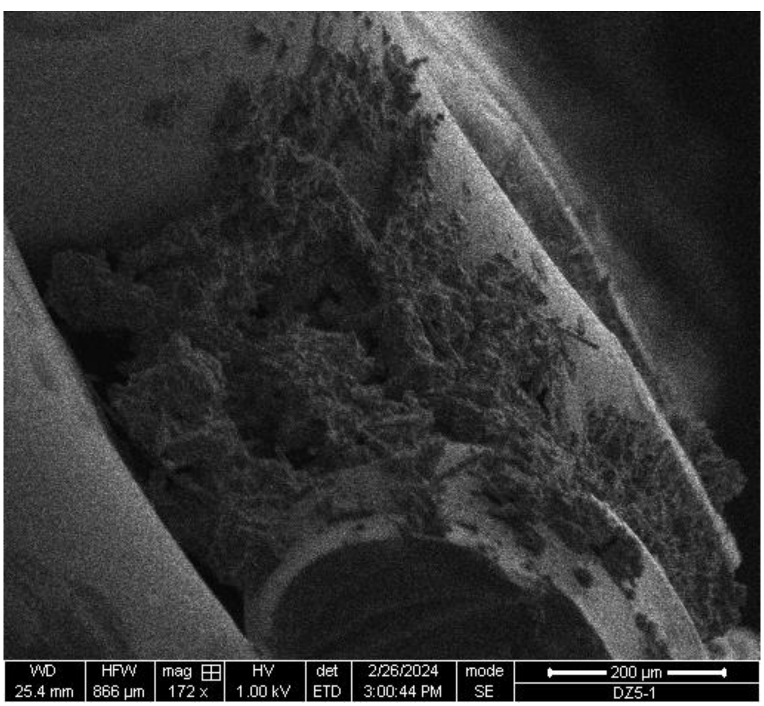

Figure 5: SEM of sample contaminated with dirt or grime prior to imaging.

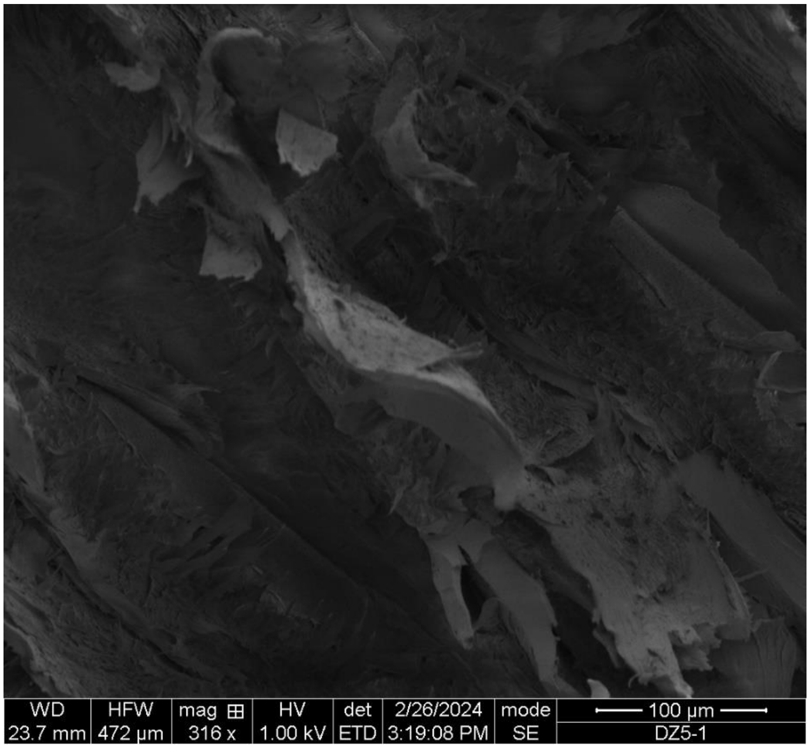

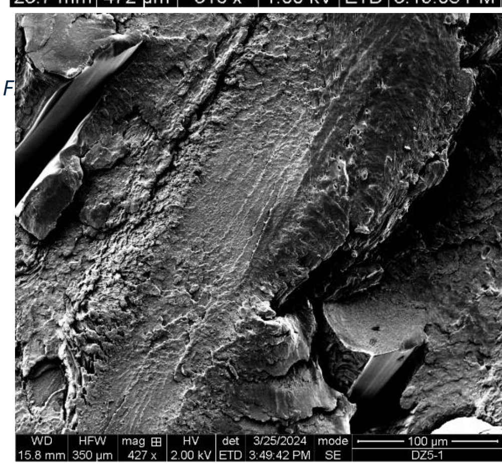

Figure 8: Close in view of breakage on a regular sample breakage surface.

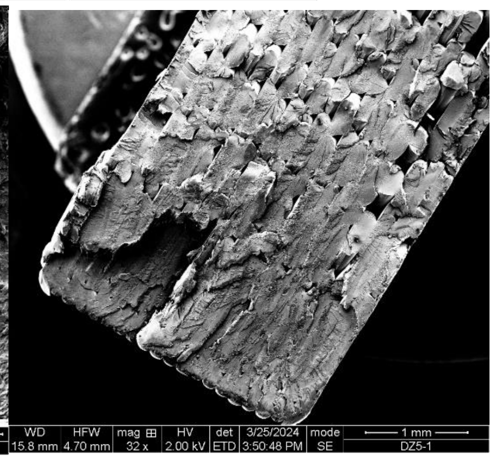

Figure 7: View of a section of regular breakage surface under SEM imaging.

2.4 Testing Apparatus

An Instron 5969 testing machine was utilized with the tensile jaws and Bluehill3 software to control the machine and record force used along with video extensometer data. A Zeiss ARAMIS adjustable DIC utilizing GOM Correlate control software was used for DIC imaging for DIC samples which was correlated to the Bluehill stress data gathered during data analysis via the start of the sample testing. A testing procedure was developed for the Bluehill software utilizing the video extensometer for gauge length extension rate feedback control for samples performed with the video extensometer, a second testing procedure was developed that utilized the testing frame extension for extension rate control as DIC software extension feedback was unavailable.

Chapter 3: Testing

3.1 Hypothesis

The hypothesis tested is that there are mechanical properties of Ultem 9085 that will be measurably influenced by changing the bead width and height of additive manufacturing. The change in bead profile can also change the geometrical characteristics of how fully the deposited beads fill the modeled space and thus the porosity and density of the part. In the analysis the weight of samples will also be considered to see if it is a better method to estimate properties.

The differing orientations of beads for different infill patterns will likely have different responses to changes in the bead profile. The XY infill pattern for example has all of the beads aligned with the stress direction, because of this the fusion area of the beads would theoretically not deflect relative to the deflection of the bead material. For the XY infill pattern any change in modulus or load capacity would be due to factors such as changes in surface or internal stresses along the beads changing due to geometric bead changes causing changes in other factors such as material cooling, this is estimated by the author to not be measurable within the scale of the samples in this thesis. The change in density is likely to provide a difference in modulus though if porosity is not accounted for in the cross sectional area of the sample, the density change would also be likely to cause an increase in overall load capacity and if not accounting for porosity an increase in tensile strength.

In the YX samples it is estimated that the effect of changing the bead geometry will induce too small of an effect in the modulus to be measured in this study. The stress is almost entirely through the bead fusion areas with no aligned beads. Changing the bead geometry will likely lead to a change in density which would change the minimum bead-bead fusion area and greatly affect the load carried showing a change in load for sample weight.

For the +- 45 degree infill pattern samples it is estimated that we will see a measurable impact on both the load and the modulus when varying the weight of the samples. The bead in these samples will both greatly vary in fusion area between beads and the beads themselves will be carrying load along the bead. This should give us both a change in stiffness as the beads will have a change in fusion area that experiences shear and a change in the porosity of the loaded cross section. This is estimated to demonstrate both an observable change in modulus and change in load, however the author is unsure if there will be any noticeable effects causing this besides the change in density.

3.2 Testing Standards

Testing was performed for ASTM D638 standards[25] with the notable deviation of having not machined the sample finish. This was done as the machining would have removed the perimeters or even infill bead at the "overlap" which is the intersection between the infill and the perimeter and includes the print bead turning around. Removing this perimeter and overlap would remove the path the stresses through the bead flows and would make these samples less characteristic of parts manufactured within reasonable scaling to these samples where one could reasonably assume that stress would continue to flow along the print bead.[12] The XY orientation samples were printed without perimeters as they would not be changed from the infill pattern.

Samples were designed for ASTM D638 Type 1 samples and modeled for 3mm thickness, individual sample thickness experienced minor variation due to layer height approximations and additional variation in under or over extruded samples. Sample thickness was not machined to uniformity to avoid impacting bead uniformity, individual sample thickness was measured with calipers and accounted for during data analysis in chapter 4. Samples were allowed time to stabilize at room temperature whenever preceding storage temperature may have had difference from room temperature specified for testing in ASTM D618.[26]

3.3 Testing Difficulties

The testing apparatus was found to need occasional cleaning of any previous sample residue notably in the knurling on the jaw faces along with periodic lubrication of the jaw-vice faces with molykote g-n paste. During DIC testing it was notably difficult to get a proper extension rate due to the lack of feedback for gauge length instead of overall extension length when utilizing the frame extension instead of the gauge extension, the values were modified to reduce the timeframe required to test but in order to keep machine behavior from hastening faster than allowable extension for some samples these samples took significantly longer to test than the non-DIC samples took. The longer sample time was not noted to demonstrate the plateauing load associated with sample creep strain. A longer sample time for the DIC also increased the data requirements as DIC is very data intense.

There were some instances of the testing apparatus "losing" the targets when utilizing the video extensometer. This would cause a testing error and is noted in the data analysis, these samples were re-attempted for testing until breakage occurred and noted to not being included in currently analyzed data.

Chapter 4: Results

4.1 Initial Analysis

The results were first separated by sample sets that were not observed to have any flaws present prior to testing. These were formed into a table of values then plotted for the Young's modulus based on layer height and then the weight. The samples were also plotted for the load at break to determine the sample's overall strength and make observations if the sample's strength did not change in the same manner as the elasticity. The results were color coded according to which nozzle diameter was utilized for the data set with blue used for 0.4mm and orange for 0.8mm, files provided by an industry partner that were utilized for their material certification was also plotted in green but was excluded from analysis for correlation.

This procedure was repeated to include sample sets with flaws in only one or two of the samples with the flawed samples removed from the analysis to check if the data remains consistent whenever flawed products are removed. With this procedure the presumption would be that the more effect a variable has on the tested properties the larger the slope in a linear regression of that data would be, the coefficient of determination would then be correlated to how reliably the regression could predict these properties when changing these variables.

0.4mm			
Layer height	Modulus	weight	load
0.25	2449.968	9.35	2255.216
0.1	2203.087	9.175	2149.786
0.2	2246.698	9.675	2405.833
0.2	2506.951	9.675	2515.371
0.8mm			
Layer height	Modulus	weight	load
0.55	2284.796	9.775	2509.611
Provided file			
Layer height	Modulus	weight	load
0.25	2241.147	9.1	2479.009

Table 1: Table of values for initial analysis of sample sets without any defects noted in entire set for +- 45 degree infill pattern samples.

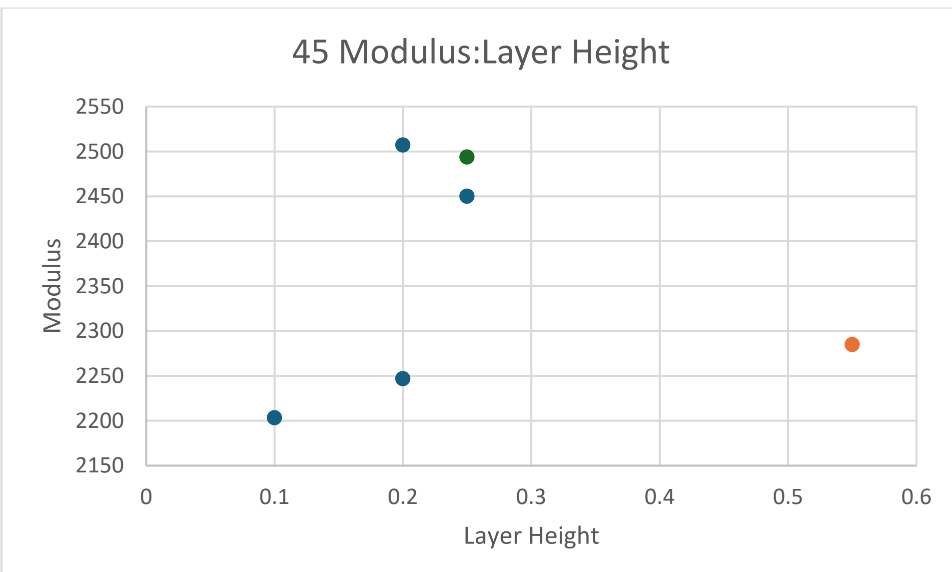

Figure 9: plot of Young's Modulus by sample layer height for 45 degree infill sample sets with no observed flaws in the entire set.

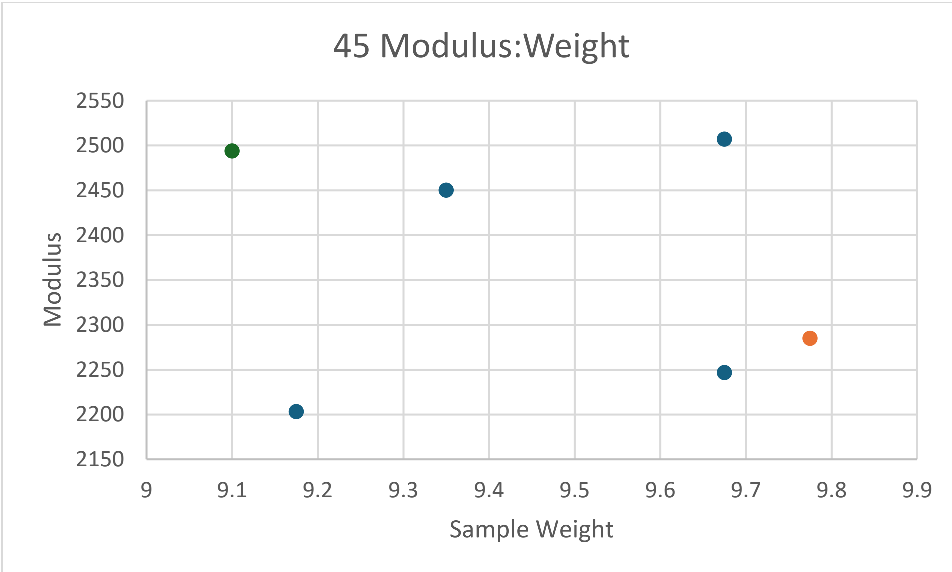

Figure 10: Plot of Young's Modulus by average sample weight for 45 degree infill sample sets with no observed flaws in the entire set.

The +/- 45 degree samples did show a correlation between the bead width and height with increasing modulus for increasing bead size. It was interesting to note that the modulus seemed to start back at a lower point for the 0.8mm nozzle size however this may be due to a small number of sample sets for 0.8mm nozzle size. The modulus not seeming to be correlated to the weight of the sample sets was also particularly interesting due to the presumption the author had that the deposition bead size would impact the modulus in part due to the increased area of fusion between the beads that is put into shear.

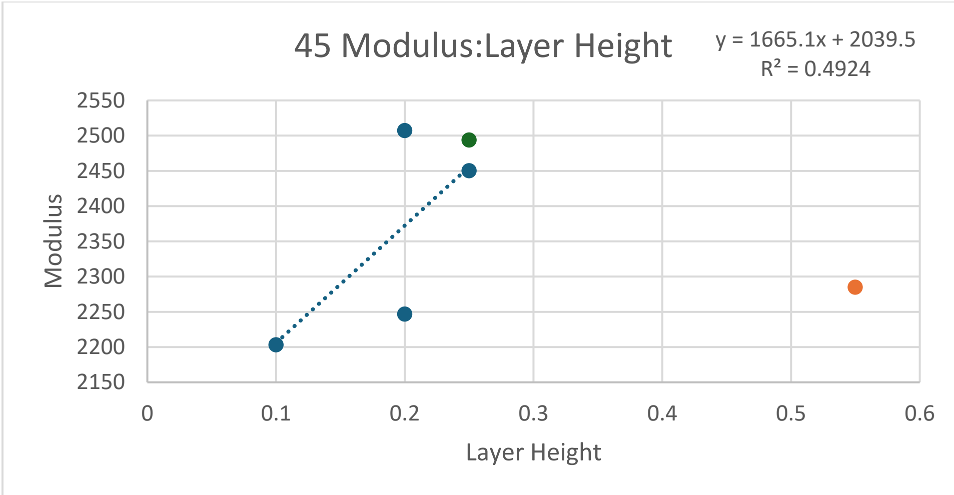

Figure 11: Excel linear regression for Young's Modulus by sample layer height for 45 degree infill sample sets with no observed flaws in the entire set.

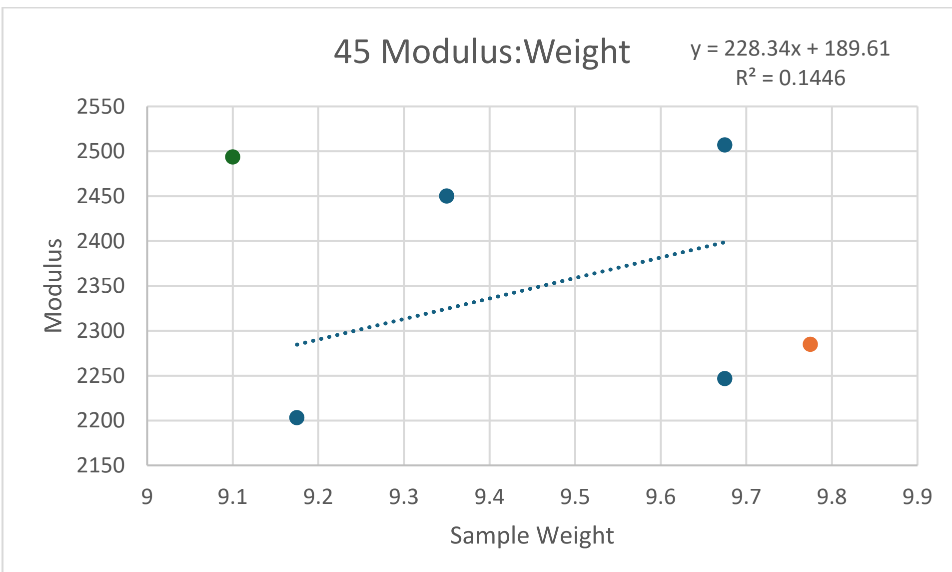

Figure 12: Excel linear regression for Young's Modulus by average sample weight for 45 degree infill sample sets with no observed flaws in the entire set.

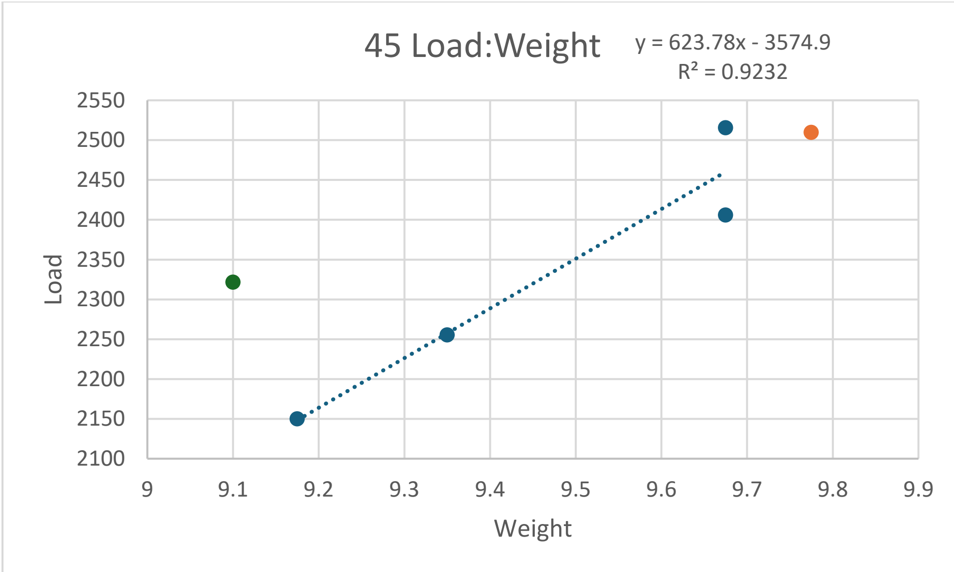

Figure 13: plot of load by average sample weight for 45 degree infill sample sets with no observed flaws in the entire set.

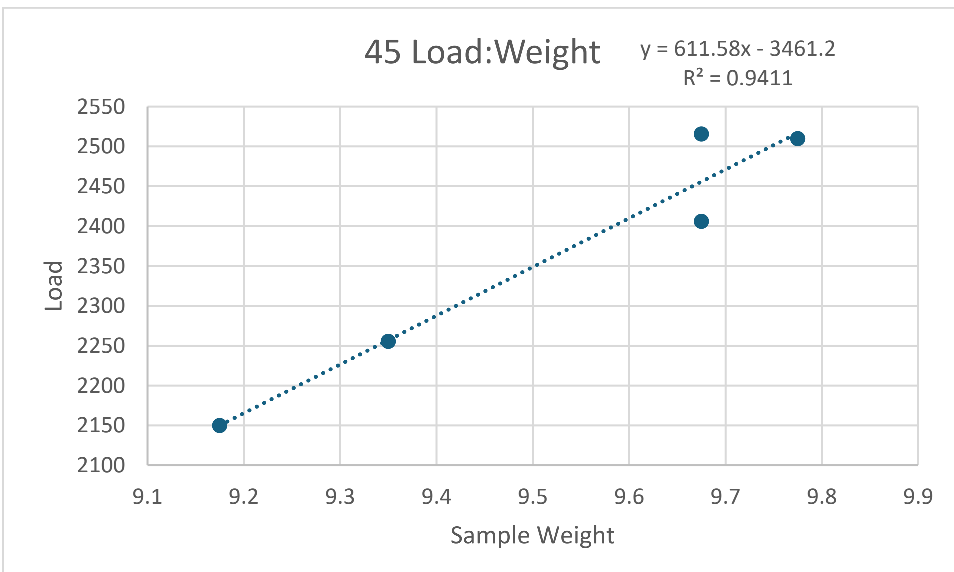

Figure 14: plot of load by average sample weight for 45 degree infill sample sets with no observed flaws in the entire set with 0.8mm nozzle and 0.4mm nozzle data combined.

Analysis via a line of best fit for the Young's modulus is noted to have a low coefficient of determination for the comparison to weight, the coefficient is much higher for the layer height but is still not high enough to conclude that this plot adequately describes the relationship. The load at break for the samples when plotted to the weight of the sample was noted to have a very high coefficient of determination despite the weight of the samples showing very little correlation to the modulus of the samples. When adding the 0.8mm data point to the linear regression the coefficient of determination rose even higher. The author notes that the change in the elasticity was also an upwards trend however with the current data size was not nearly as reliable to estimate modulus.

To determine statistical significance a one way analysis of variance (ANOVA) test was performed in order to confirm that there is an observed relationship, even if the linear regressions performed are not adequate for describing the relationship. The one way ANOVA for both modulus and load showed a P-value of less than .01 with F values higher than 5 indicating that there is a significant change between groups.

Anova: Single Factor	Modulus					
SUMMARY						
Groups	*Count*	*Sum*	*Average*	*Variance*		
height 0.25	6	14699.81	2449.968177	28123		
height 0.1	4	8812.35	2203.087438	11350		
height 0.2	4	8986.792	2246.698013	11673		
Height 0.2	4	10027.8	2506.951113	6805.7		
ANOVA						
Source of Variation	SS	df	MS	F	P-value	F crit
Between Groups	284658.3	3	94886.09253	5.7731	0.008737028	3.3439
Within Groups	230104.2	14	16436.01333			
Total	514762.5	17				

Table 2: Table of results from ANOVA analysis for +- 45 degree infill pattern modulus for sample sets with no flaws observed in the sample set.

Anova: Single Factor		Load				
SUMMARY						
Groups	*Count*	*Sum*	*Average*	*Variance*		
height 0.25	6	13531.29	2255.216	30415.5815		
height 0.1	4	8599.145	2149.786	2649.95588		
height 0.2	4	9623.331	2405.833	7701.44036		
Height 0.2	4	10061.48	2515.371	13623.7119		
ANOVA						
Source of Variation	*SS*	*df*	*MS*	*F*	*P-value*	*F crit*
Between Groups	323051	3	107683.7	6.73013602	0.004855	3.343889
Within Groups	224003	14	16000.23			
Total	547054	17				

Table 3: Table of results from ANOVA analysis for +- 45 degree infill pattern load for sample sets with no flaws observed in the sample set.

The combination of the ANOVA showing a significant change in the data set and the high coefficient of determination for the load-weight plot would suggest that this is the real relationship between these properties, albeit at a small sample size. The moderate coefficient of determination for the modulus and layer height with the significant change shown by the ANOVA would suggest that this is where the relationship between the properties is but this relationship would need significant refinement to confirm it is the relationship and become a valid approximation.

0.4mm			
Layer height	Modulus	weight	Load
0.15	2401.166	8.25	2615.591
0.25	2437.902	8.725	2550.103
0.15	1838.083	7.4	2195.24
0.1	2322.204	8.6	2220.699
0.25	4488.379	8.75	2686.496
0.2	2145.947	8.5	2439.479
0.2	2489.517	8.5	2683.427
0.15	2012.282	8.4	2602.795
0.8mm			
Layer height	Modulus	weight	load
0.25	2093.086	8.85	2970.291
0.2	2050.341	8.3	2713.305
0.35	2046.836	8.625	2252.482
0.55	2224.536	8.9	2791.38
0.5	1968.931	8.175	2683.196
0.55	2035.657	8.8	2563.445
0.3	2092.256	9	2925.753
0.4	2231.279	8.725	2778.997
0.45	2501.059	8.9	2848.05
provided			
Layer height	Modulus	weight	load
0.25	2355.162	10.55	2682.009

Table 4: Table of values for initial analysis of sample sets without any defects noted in entire set for XY infill pattern samples.

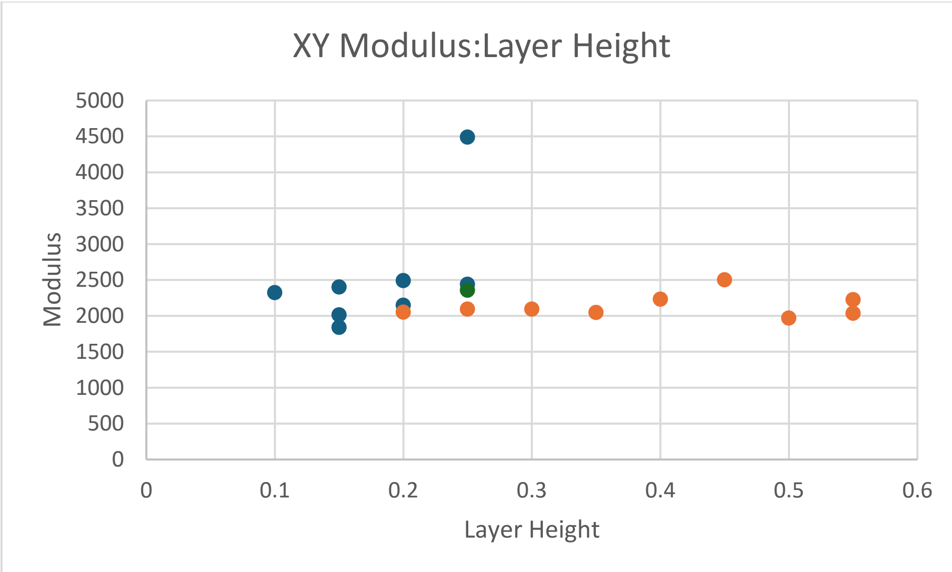

Figure 15: plot of Young's Modulus by sample layer height for XY orientation infill sample sets with no observed flaws in the entire set.

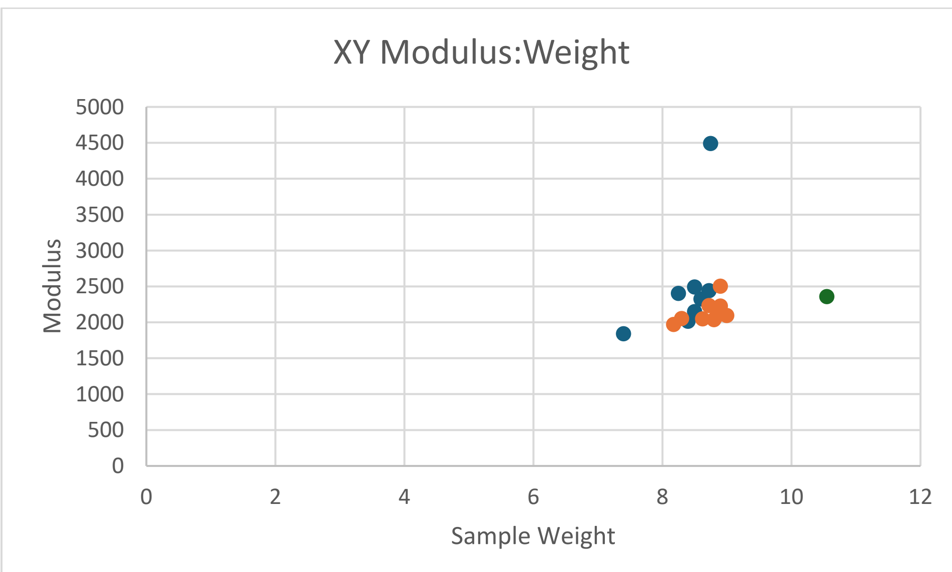

Figure 16: plot of Young's Modulus by average sample weight for XY orientation infill sample sets with no observed flaws in the entire set.

The most surprising of these results was the modulus for the XY orientation showing little change across layer height change. The author initially thinks this may be due to either a lack of the software accounting for porosity changing the cross sectional area of the sample or a lack of inter-bead forces or interactions when the sample is put into tension as the XY orientation will act as tension along the bead direction. This lack of shear stresses across the bead-bead interface would suggest that the changes in modulus seen in the +/- 45 degree sample sets is primarily due to effects on the bead interface during manufacturing. The modulus is noted to have a slight correlation to increasing with the sample weight.

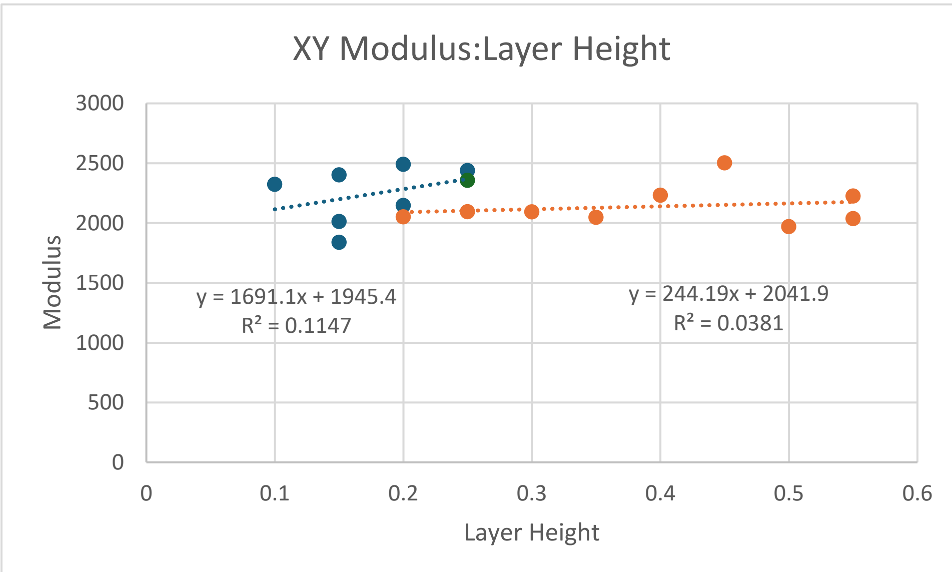

Figure 17: Excel linear regression of Young's Modulus by sample layer height for XY orientation infill sample sets with no observed flaws in the entire set.

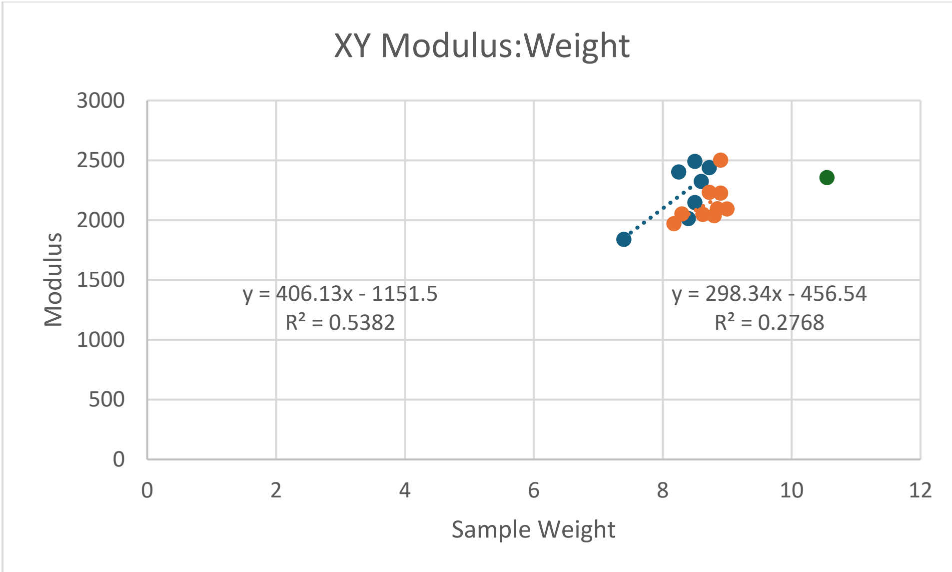

Figure 18: Excel linear regression of Young's Modulus by sample layer height for XY orientation infill sample sets with no observed flaws in the entire set.

The modulus-layer height for XY orientation samples analyzed via line of best fit was noted to have low coefficients of determination. Analyzing with both nozzles data grouped together did not yield a better relationship. The load-weight relationship of the XY analyzed via line of best fit did show a positive correlation in the same manner that the modulus showed a correlation however both of these were not a reliable method to estimate the modulus.

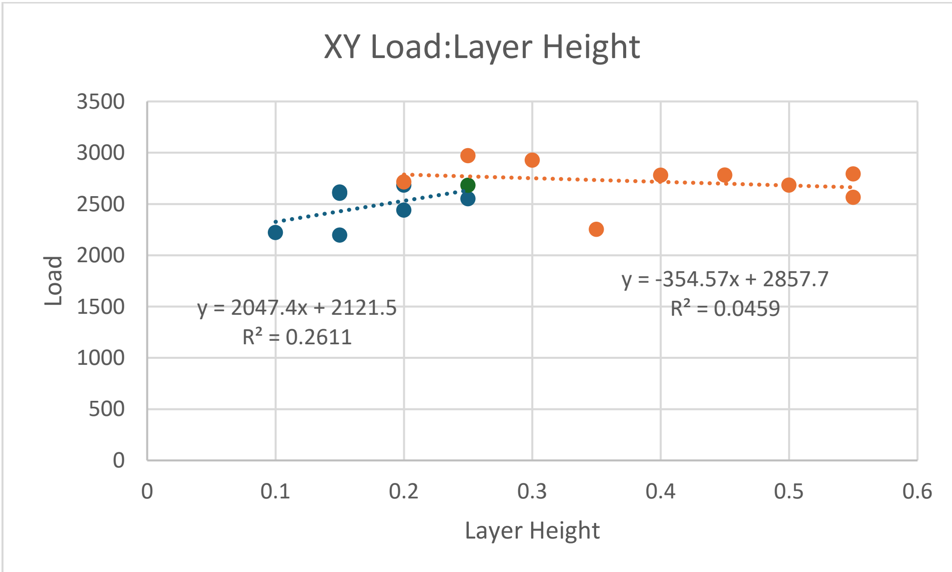

Figure 19: Excel linear regression of load by sample layer height for XY orientation infill sample sets with no observed flaws in the entire set.

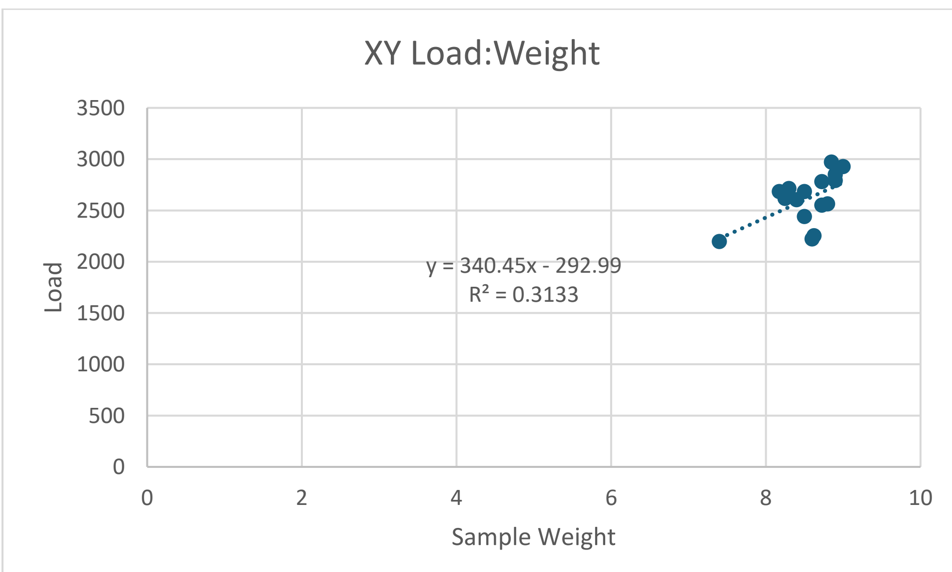

Figure 20: Excel linear regression of load by average sample weight for XY orientation infill sample sets with no observed flaws in the entire set.

Anova: Single Factor		Modulus 0.4mm				
SUMMARY						
Groups	*Count*	*Sum*	*Average*	*Variance*		
0.15	2	4802.331	2401.166	6590.251		
0.25	4	9751.61	2437.902	35988.64		
0.15	4	7352.332	1838.083	1666.125		
0.1	3	6966.612	2322.204	10945.61		
0.25	4	17953.52	4488.379	46617.41		
0.2	4	8583.787	2145.947	21687.54		
0.2	4	9958.066	2489.517	54479.59		
0.15	4	8049.129	2012.282	2267.425		
ANOVA						
Source of Variation	*SS*	*df*	*MS*	*F*	*P-value*	*F crit*
Between Groups	19121252	7	2731607	111.0406	3.81E-15	2.487578
Within Groups	516601.7	21	24600.08			
Total	19637854	28				

Table 5: Table of results from ANOVA analysis for XY infill pattern modulus for sample sets with 0.4mm nozzle and no flaws observed in the sample set.

Anova: Single Factor		Modulus 0.8mm				
SUMMARY						
Groups	*Count*	*Sum*	*Average*	*Variance*		
0.25	4	8372.344	2093.086	10900.53		
0.2	4	8201.363	2050.341	7620.478		
0.35	4	8187.346	2046.836	9759.907		
0.55	4	8898.144	2224.536	59402.69		
0.5	4	7875.722	1968.931	1641.224		
0.55	4	8142.629	2035.657	10623.32		
0.3	4	8369.025	2092.256	2464.872		
0.4	4	8925.115	2231.279	5789.409		
0.45	4	9189.383	2297.346	11886.8		
ANOVA						
Source of Variation	*SS*	*df*	*MS*	*F*	*P-value*	*F crit*
Between Groups	384887.6	8	48110.95	3.60564	0.005691	2.305313
Within Groups	360267.7	27	13343.25			
Total	745155.3	35				

Table 6: Table of results from ANOVA analysis for XY infill pattern modulus for sample sets with 0.8mm nozzle and no flaws observed in the sample set.

The results of an ANOVA for the modulus for both nozzles does have F values higher than 3 with P values below .01 which indicates a significant difference in values for the data, particularly for the 0.4mm nozzle having an F value of 111. This would suggest there is a relationship between the modulus and either the layer height or the weight, with the coefficient of determination being much higher for the weight relationship this suggests the sample weight influences the sample modulus for XY orientation samples although the coefficient is low enough that the relationship needs refining before it could be confirmed that this regression is the relationship and be considered useful.

Anova: Single Factor		0.4mm Load				
SUMMARY						
Groups	*Count*	*Sum*	*Average*	*Variance*		
0.15	2	5231.182	2615.591	765.1348		
0.25	4	10200.41	2550.103	75231.04		
0.15	4	8780.958	2195.24	9945.238		
0.1	3	6662.097	2220.699	8329.965		
0.25	4	10745.98	2686.496	75423.37		
0.2	4	9757.917	2439.479	97564.57		
0.2	4	10733.71	2683.427	9368.401		
0.15	4	10411.18	2602.795	149571.4		
ANOVA						
Source of Variation	*SS*	*df*	*MS*	*F*	*P-value*	*F crit*
Between Groups	972911.8	7	138987.4	2.300504	0.065949	2.487578
Within Groups	1268737	21	60416.06			
Total	2241649	28				

Table 7: Table of results from ANOVA analysis for XY infill pattern load for sample sets with 0.4mm nozzle and no flaws observed in the sample set.

Anova: Single Factor		0.8mm Load				
SUMMARY						
Groups	*Count*	*Sum*	*Average*	*Variance*		
0.25	4	11881.16	2970.291	2627.057		
0.2	4	10853.22	2713.305	6485.842		
0.35	4	11265.6	2816.399	1886.673		
0.55	4	11165.52	2791.38	1576.992		
0.5	4	10732.78	2683.196	124.852		
0.55	4	10253.78	2563.445	34304.6		
0.3	4	11703.01	2925.753	5077.204		
0.4	4	11115.99	2778.997	15512.71		
0.45	4	11126.96	2781.741	11826.14		
ANOVA						
Source of Variation	*SS*	*df*	*MS*	*F*	*P-value*	*F crit*
Between Groups	478504.3	8	59813.04	6.777932	7.12E-05	2.305313
Within Groups	238266.2	27	8824.674			
Total	716770.5	35				

Table 8: Table of results from ANOVA analysis for XY infill pattern load for sample sets with 0.8mm nozzle and no flaws observed in the sample set.

The ANOVA performed for the load in the XY samples did not find the testing to be as significantly different as the modulus performed. The load variation found for the 0.8mm nozzle would be considered significantly different but the data for the 0.4mm nozzle is less convincing. Between the results of this ANOVA and the low coefficients of determination it cannot be confirmed that either are the relationship between load and printing parameters however the coefficient of determination being higher for the sample weight would suggest this parameter to be the parameter to explore for this relationship.

The YX samples are loaded almost entirely across bead-bead fusion as the gauge length is only one perimeter filled with fused layers perpendicular to the applied stress. With this understanding the effect of the bead changing would presumably show almost entirely changes in effects on the bead-bead fusion, the fusion between beads is understood to be the weakest aspect of polymers manufactured with fused deposition modeling[11-13, 16] and thus effects seen here are expected to be smaller than effects seen in other orientations if the effects are noticeable at all.

0.4mm			
Layer height	Modulus	weight	Load
0.25	2190.208	9.166667	1294.31
0.25	2133.759	9.375	1418.391
0.1	2619.944	9.275	1276.44
0.2	2532.702	9.2	1268.16
0.25	2431.653	9.425	1702.258
0.15	2313.367	9.55	1006.666
Provided			
Layer height	Modulus	weight	Load
0.25	2619.944	8.966667	1755.319

Table 9: Table of values for initial analysis of sample sets without any defects noted in entire set for XY infill pattern samples.

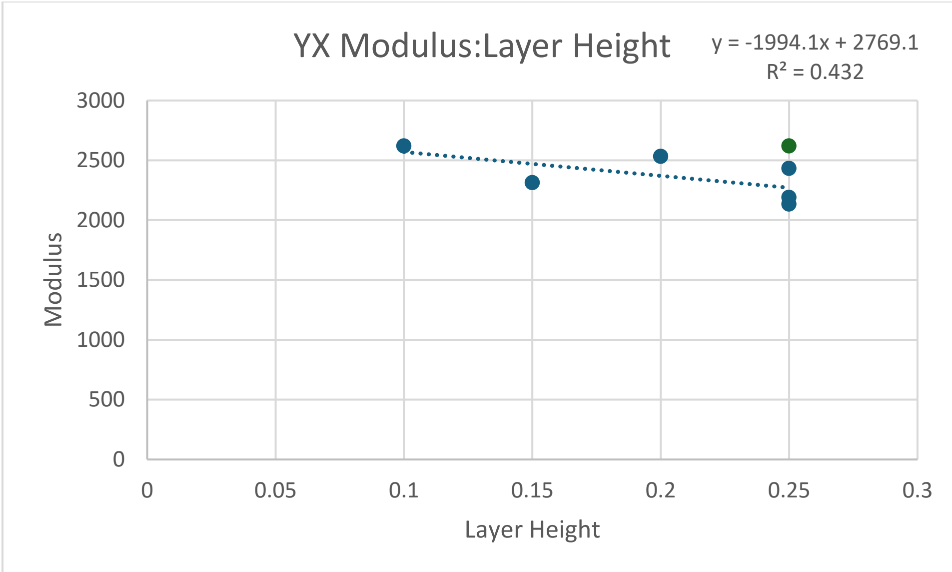

Figure 21: Plot of and Excel linear regression of Young's Modulus by sample layer height for YX orientation infill sample sets with no observed flaws in the entire set.

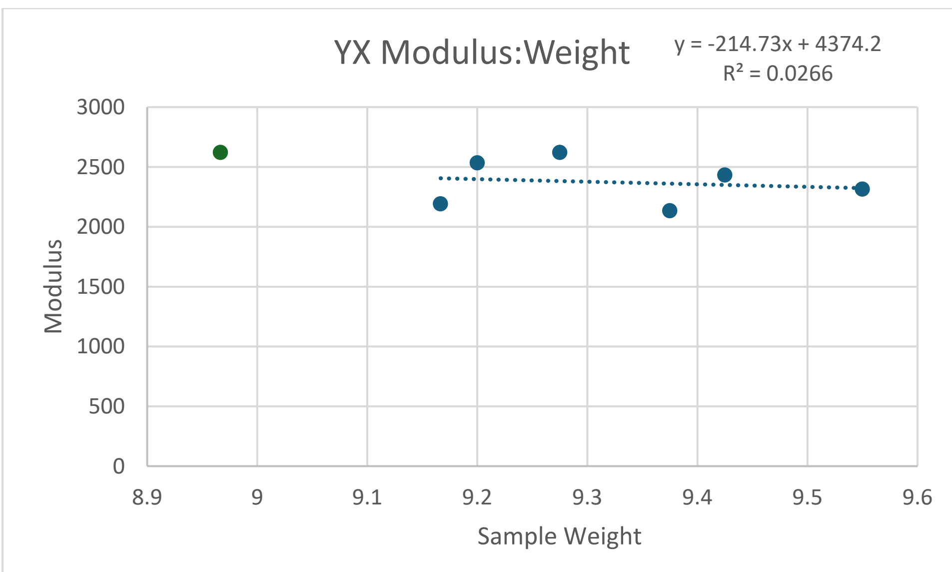

Figure 22: Plot of and Excel linear regression of Young's Modulus by average sample weight for YX orientation infill sample sets with no observed flaws in the entire set.

The YX modulus showed a moderate value that was much higher than anticipated for the coefficient of determination for the layer height however the relationship between the modulus and the layer height was a negative relationship. This would suggest that if the data is significant then increasing the bead height actually decreases the modulus and makes the material less stiff. The modulus to weight also showed a negative relationship however the relationship was much smaller with a significantly lower coefficient of determination suggesting we will likely not find this to be a significant relationship upon examining statistical significance.

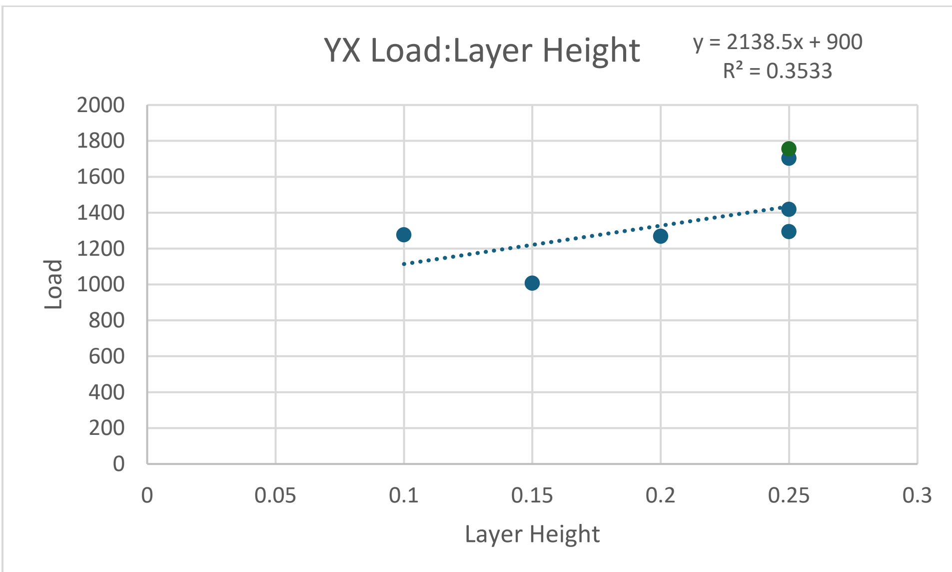

Figure 23: Plot of and Excel linear regression of load by sample layer height for XY orientation infill sample sets with no observed flaws in the entire set.

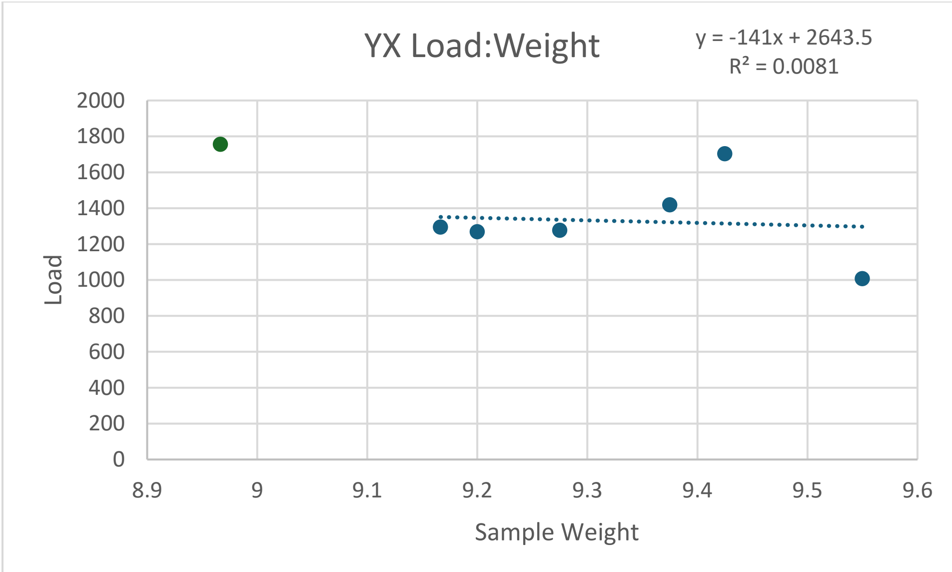

Figure 24: Plot of and Excel linear regression of load by average sample weight for XY orientation infill sample sets with no observed flaws in the entire set.

The YX load again showed a higher than expected coefficient of determination for the set and this time did show a positive increase. This is in contrast to the trends seen in other orientations where generally the material's stiffness and load have risen or fallen in the same direction even when not at the same scales. The load to weight showed similar results as the modulus to weight for this orientation as it is a much smaller relationship with a very low coefficient of determination again suggesting we will find this relationship to not be statistically significant.

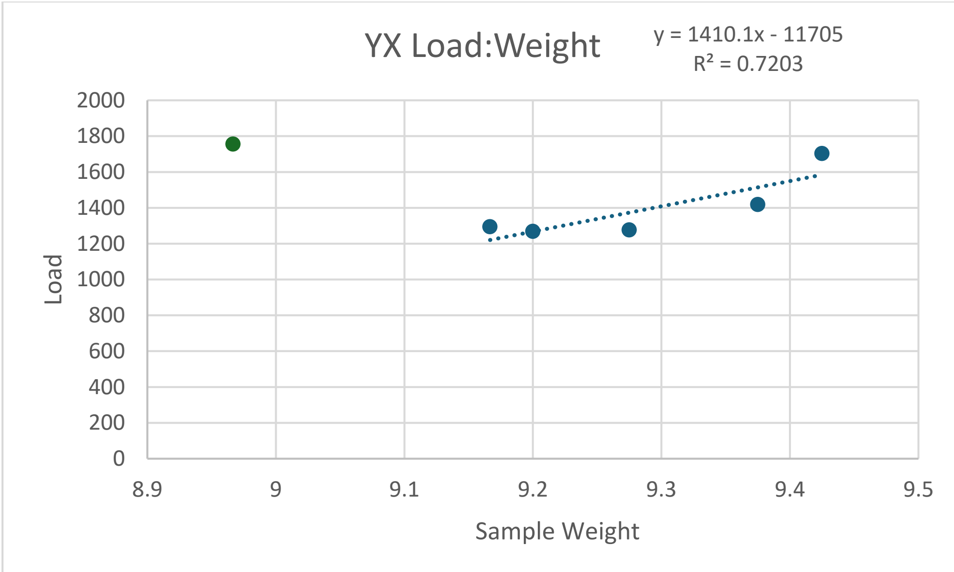

Figure 25: Plot of and Excel linear regression of load by average sample weight for YX orientation infill sample sets with studentized residual removed and no observed flaws in the entire set.

It was noticed that the highest weight data point could be an outlier and the analysis was re-ran with this data point excluded. When this was performed the analysis found a much higher coefficient of determination which would agree with the hypothesis that load is measurably affected by the sample density. This was checked against a studentized residual for the studentized Z score which at a score above 2 but below 3 did not confirm this point to be an outlier with this sample size.

std dev determination				
Load	weight	Calc load new	Residual	Z score
1294.31	9.166667	1220.916667	73.39329	0.210552
1418.391	9.375	1514.6875	-96.2969	0.276258
1276.44	9.275	1373.6775	-97.2372	0.278956
1268.16	9.2	1267.92	0.24019	0.000689
1702.258	9.425	1585.1925	117.0657	0.33584
1006.666	9.55	1761.455	-754.789	2.165351
			Studentized residual	
			348.5757	

The studentized residual was used due to the small sample size causing an outlier to skew it's own outlier analysis. This analysis by itself would not be substantial enough to definitively confirm the trendline is the relationship between these properties due to the implications of the sample size being small enough to warrant a studentized residual however it can guide further analysis and experimentation to explore this relationship as it suggests a larger sample size would find this to be an outlier.

Anova: Single Factor		Modulus				
SUMMARY						
Groups	*Count*	*Sum*	*Average*	*Variance*		
0.25	6	13141.25	2190.208	35572.05		
0.25	4	8535.037	2133.759	24913.81		
0.1	4	10479.78	2619.944	374661.7		
0.2	4	10130.81	2532.702	23101.5		
0.25	4	9726.611	2431.653	51746.87		
0.15	4	9253.47	2313.367	47946.81		
ANOVA						
Source of Variation	*SS*	*df*	*MS*	*F*	*P-value*	*F crit*
Between Groups	796205.6	5	159241.1	1.825142	0.153573	2.71089
Within Groups	1744972	20	87248.62			
Total	2541178	25				

Table 10: Table of results from ANOVA analysis for YX infill pattern modulus for sample sets with no flaws observed in the sample set.

Anova: Single Factor		Load				
SUMMARY						
Groups	*Count*	*Sum*	*Average*	*Variance*		
0.25	6	7765.86	1294.31	42425.3		
0.25	4	5673.562	1418.391	3140.795		
0.1	4	5105.761	1276.44	10258.33		
0.2	4	5072.641	1268.16	15474.41		
0.25	4	6809.033	1702.258	11165.39		
0.15	4	4026.665	1006.666	15965.29		
ANOVA						
Source of Variation	*SS*	*df*	*MS*	*F*	*P-value*	*F crit*
Between Groups	1037534	5	207506.7	10.91741	3.59E-05	2.71089
Within Groups	380139.2	20	19006.96			
Total	1417673	25				

Table 11: Table of results from ANOVA analysis for YX infill pattern load for sample sets with no flaws observed in the sample set.

The one way ANOVA for the modulus of the YX samples showed a F value below 2 with a P value over .15, between these factors and the linear regression not finding a confident relationship between the YX orientation modulus and the independent variables it is concluded that the modulus for this orientation did not demonstrate change necessary to establish a relationship. The ANOVA for the load had an F value above 10 and a P value below .01 however which would suggest that there is a significant change in the load and with the linear regression for weight, after removing outliers, showing a coefficient of determination of 0.72 there is supporting evidence that this is an area to explore with an expanded sample set needed to refine the relationship.

4.2 Reexamining Analysis for Porosity Factors

The calculations performed within the Bluehill software for the modulus utilize a cross section formed through inputs where the software is told the cross sectional measurements of the sample. The sample weights were separately recorded and input with the analysis being performed in excel, the varying sample weights compared to the sample volume could also be modeled as a porosity measurement. If we utilize the 1.34 g/cm^3[27] density of Ultem 9085 as a bulk solid material with and area of 26.23182 cm^2 multiplied by the thickness of the sample to eliminate rounding error between the model and the end print the weight of the sample if it were fully dense is found. With this the measured weight of the sample can be utilized to find the percentage of porosity and recalculate the Young's modulus utilizing the refigured cross section.

The author does note that this analysis does not work out to represent the cross section the same for the YX samples. This is due to the direction of the voids between beads being parallel to the cut direction of the cross section. This results in the cross section potentially intersecting a portion that does not contain any voids and is completely dense, or intersecting the maximum dimension of the void shapes thus being the least dense possibility.

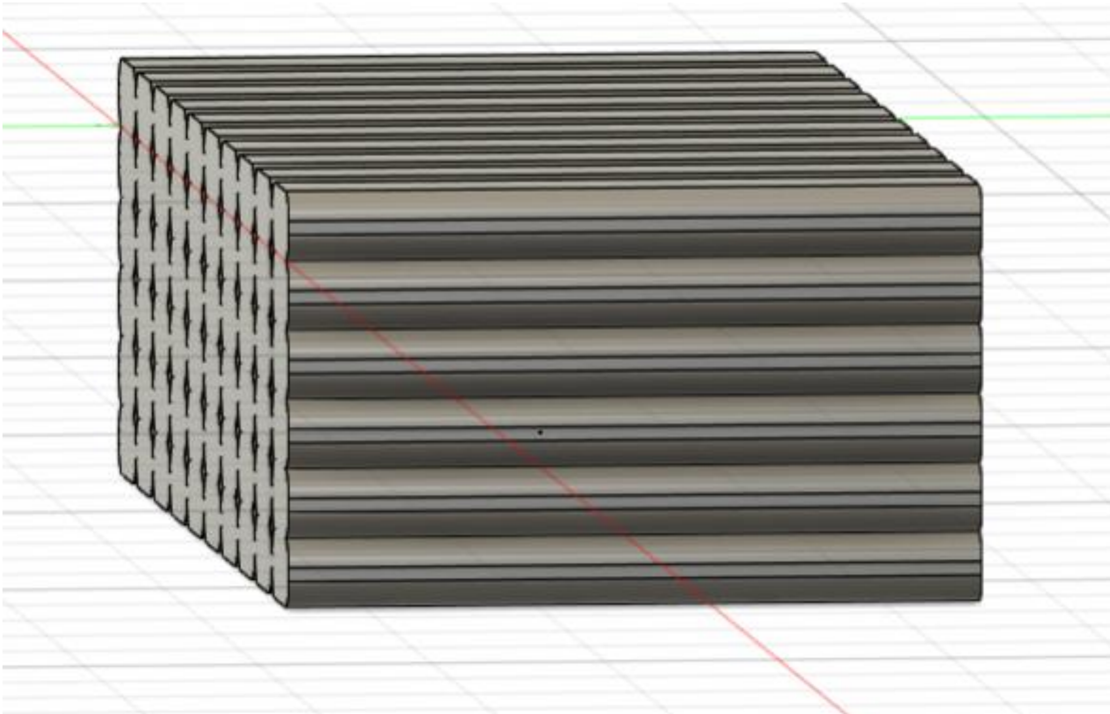

Figure 26: Fusion 360 model of YX sample cross section. This is noted to be the same as the XY infill pattern but turned 90 degrees.

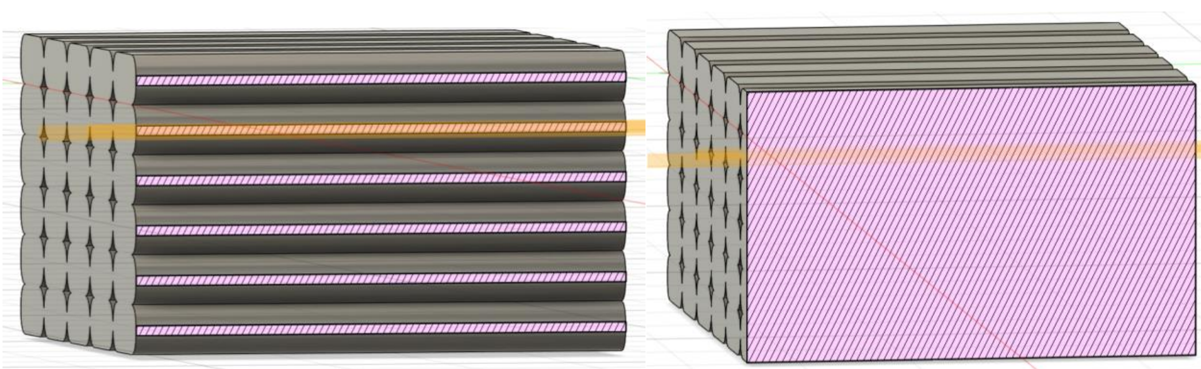

Figure 27: Fusion 360 model of cross sections taken along different points of YX sample infill pattern. The two sectional cuts shown display the changing cross sectional area between the lower contacting fused bead width edges and the near-solid contacting fused bead heights. Models are not based on any measured fused areas.

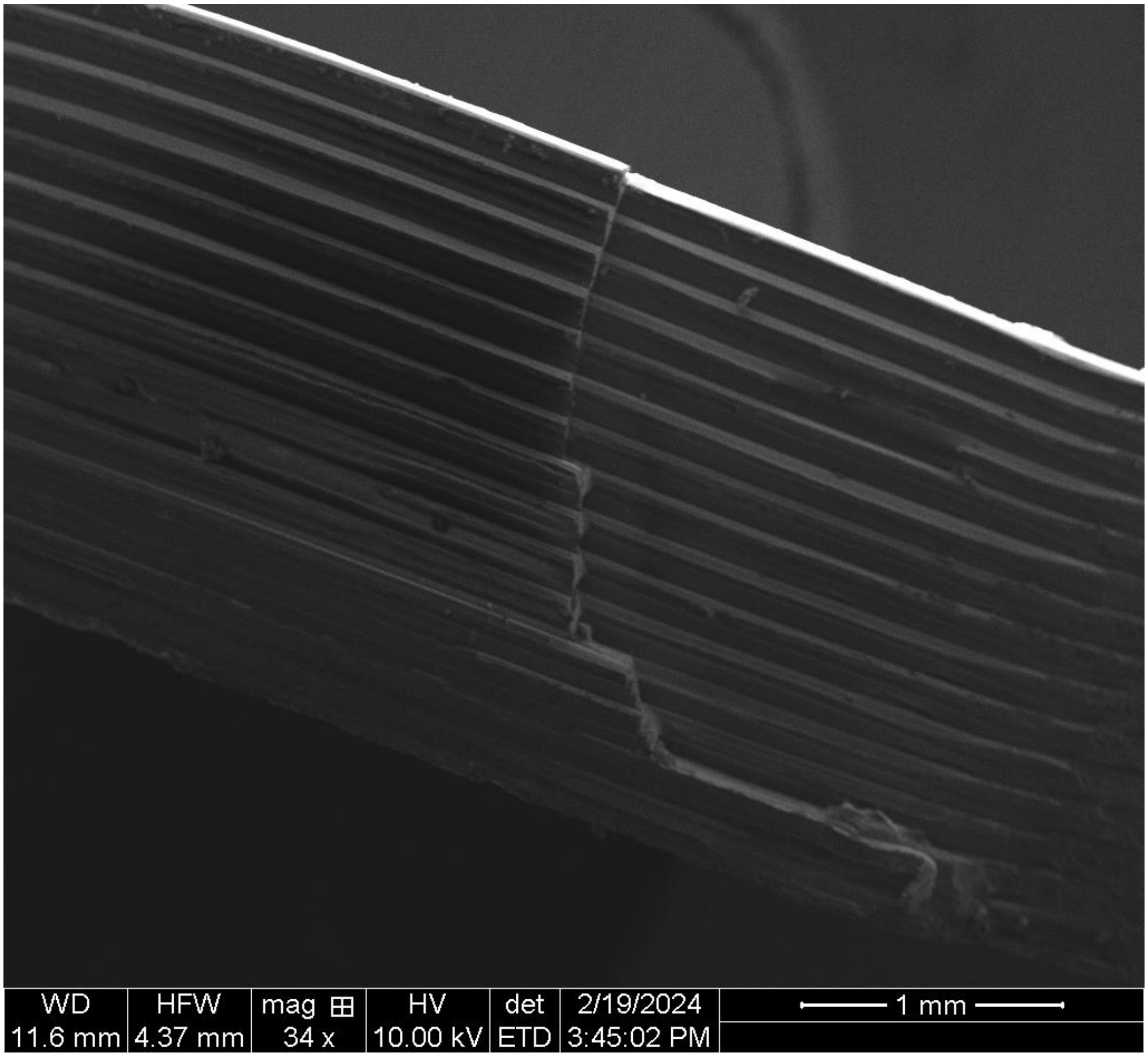

Figure 28: SEM image of sample #14 YX orientation sample break surface.

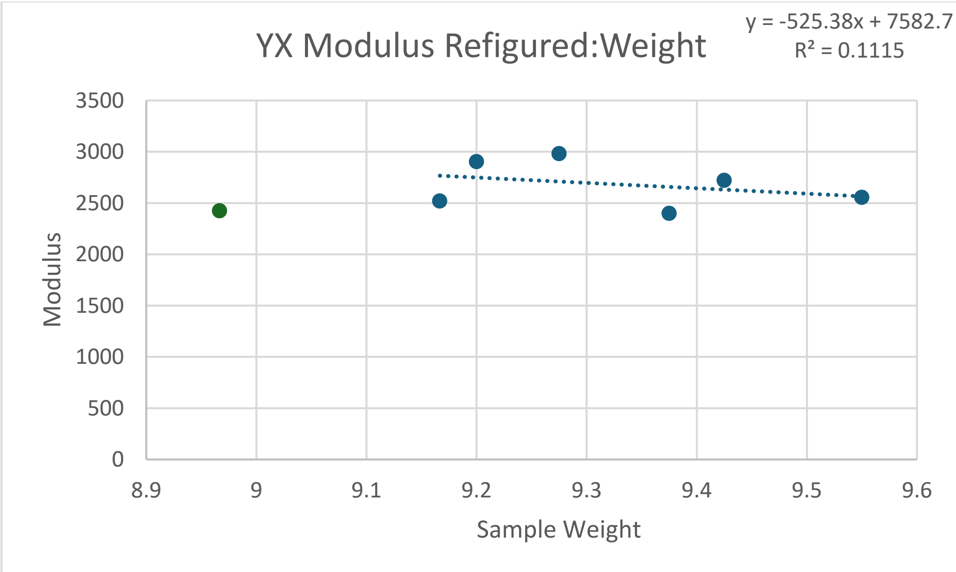

Figure 29: Plot of and Excel linear regression of modulus refigured for porosity by average sample weight for YX orientation infill sample sets with no observed flaws in the entire set.

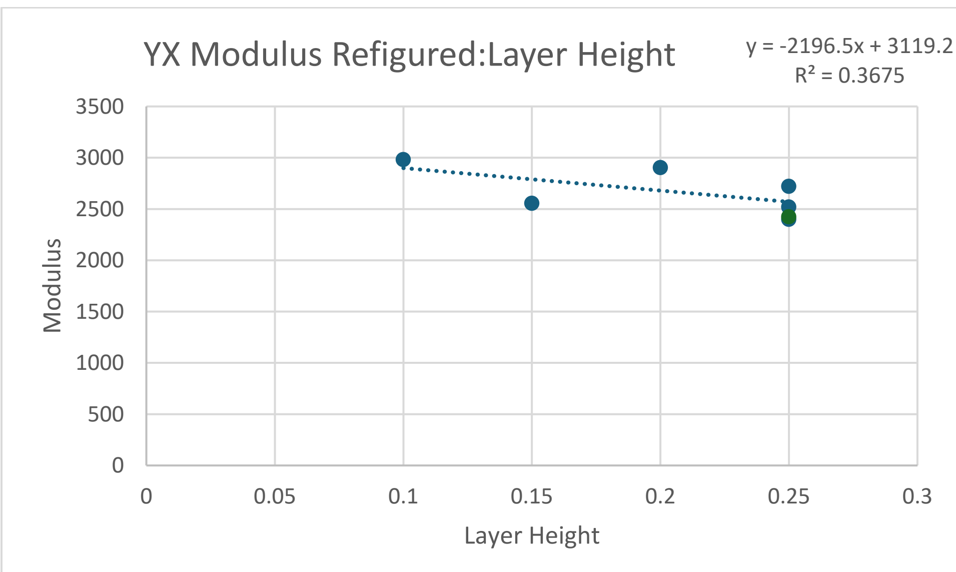

Figure 30: Plot of and Excel linear regression of modulus refigured for porosity by average sample weight for YX orientation infill sample sets with no observed flaws in the entire set.

The plots of the YX modulus accounting for porosity in the samples did show an increase in the magnitude of the relationship between modulus and weight and also had an increase of over four times the coefficient of determination, however this relationship was already a weak relationship with a very low coefficient of determination. This relationship was still notably a negative relationship. If a larger sample set with a broader range of values was performed it is possible it would demonstrate a significant change however this cannot be validated with this data. The modulus to layer height showed a stronger relationship however the coefficient of determination was already low and became slightly lower.

Anova: Single Factor						
SUMMARY						
Groups	*Count*	*Sum*	*Average*	*Variance*		
0.25	6	15118.43	2519.739	47511.51		
0.25	4	9596.528	2399.132	24423.44		
0.1	4	11926.19	2981.548	511290.1		
0.2	3	7270.19	2423.397	59372.3		
0.25	4	11612.8	2903.199	31086.34		
0.15	4	10219.96	2554.99	62388.77		
ANOVA						
Source of Variation	*SS*	*df*	*MS*	*F*	*P-value*	*F crit*
Between Groups	1229601	5	245920.1	2.082334	0.1125	2.740058
Within Groups	2243868	19	118098.3			
Total	3473469	24				

Table 12: Table of results from ANOVA analysis for YX infill pattern load for sample sets with no flaws observed in the sample set.

The results of the ANOVA for the refigured modulus for the YX samples showed similarly poor F and P values as the ANOVA for the initially considered modulus and reinforce the conclusion that the YX infill pattern did not display a significant change in modulus.

For the XY samples the cross section will, provided the sample is uniform as will be assumed in this analysis, capture the same porosity of cross section at all points along the gauge length. Given that the XY analysis initially performed did not have the combination of strong relationships and high coefficient of determination between the variable and the reexamined property this may yield a more significant result or simply also find this test uncertain for the reexamined property.

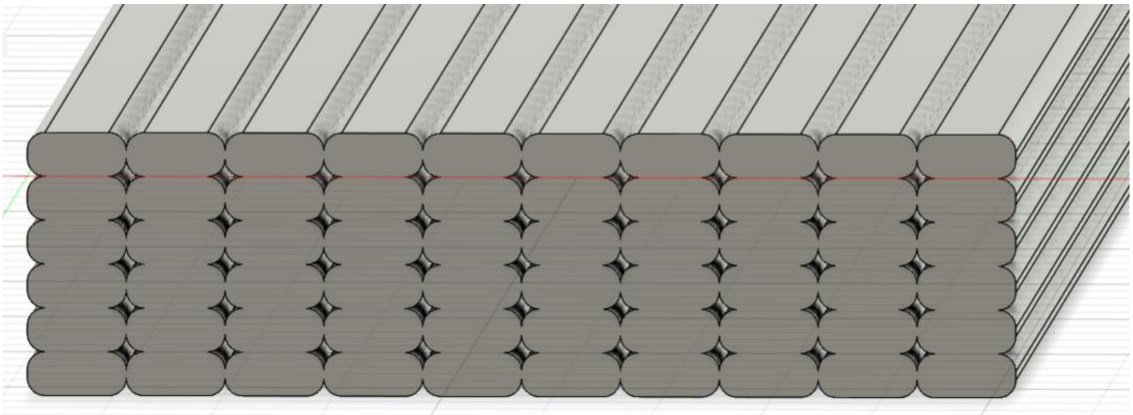

Figure 31: Fusion360 model depicting infill pattern of XY infill samples. This is the same as the cross section.

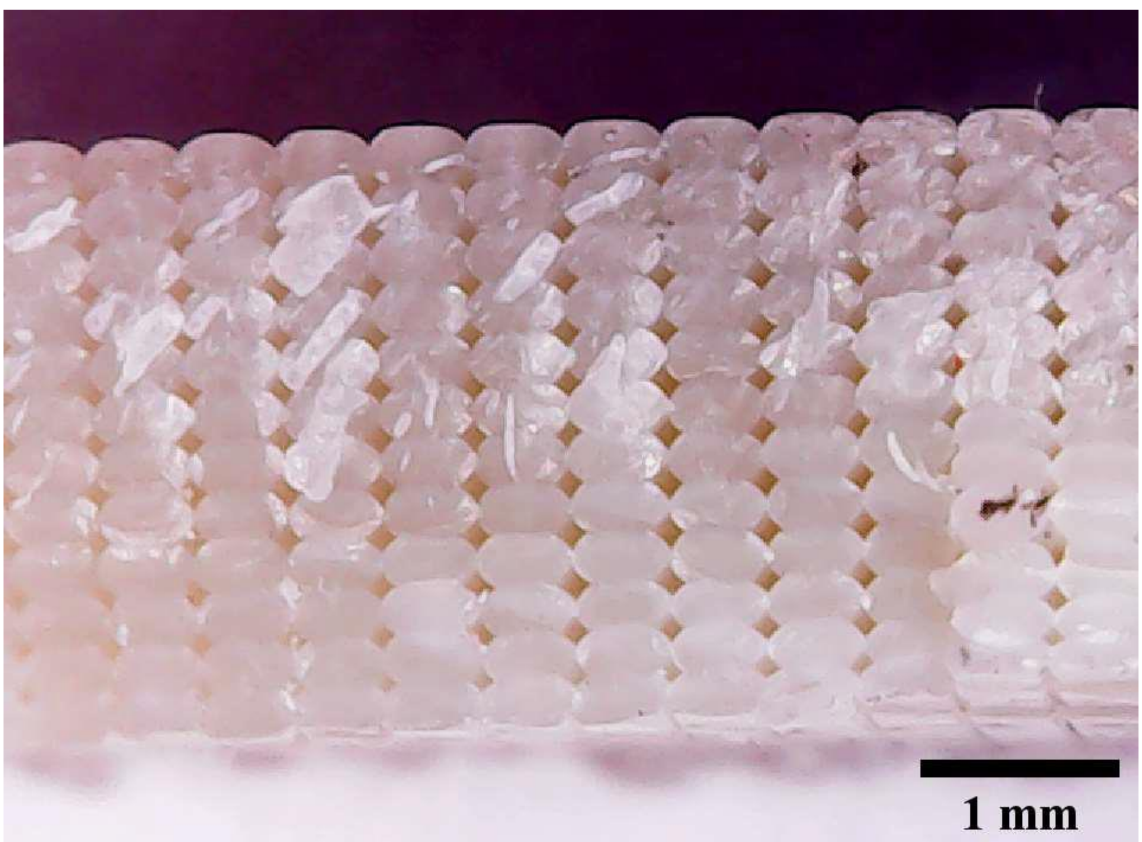

Figure 32: Image of cross section of an XY orientation sample of Ultem 9085 by Kuzmina et, al.[11]

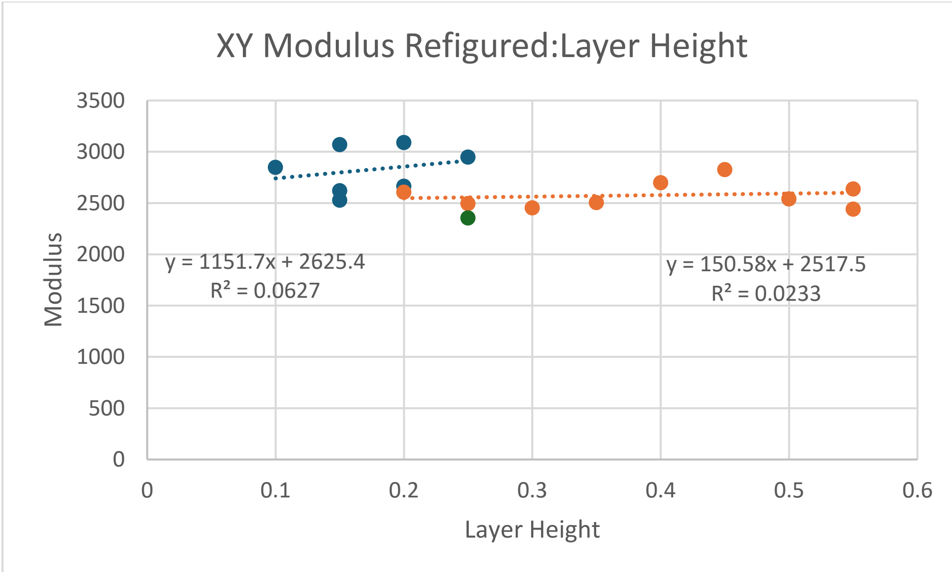

Figure 33: Plot of and Excel linear regression of modulus refigured for porosity by layer height for XY orientation infill sample sets with no observed flaws in the entire set.

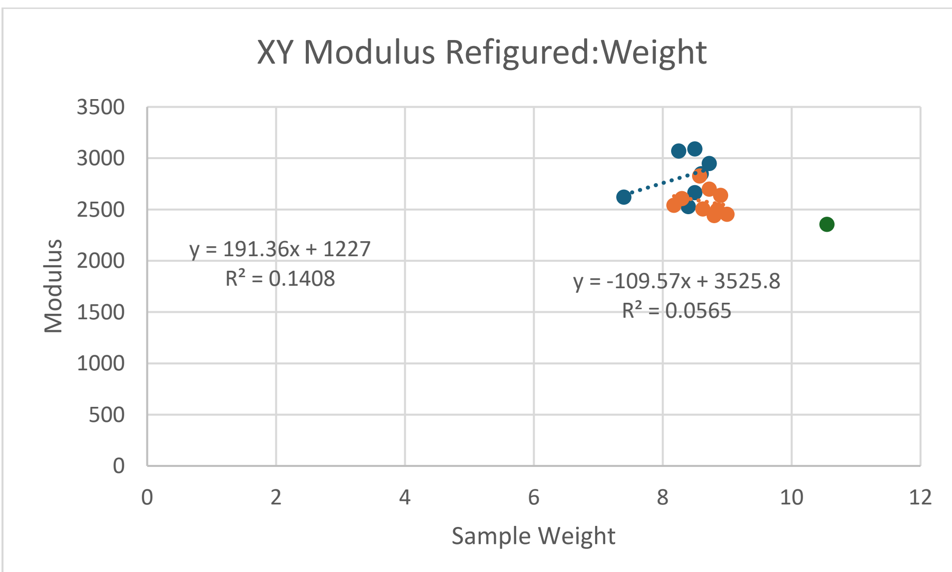

Figure 34: Plot of and Excel linear regression of modulus refigured for porosity by average sample weight for XY orientation infill sample sets with no observed flaws in the entire set.

The plots for the XY modulus and sample weight when accounting for porosity show a weaker relationship both in terms of magnitude of relationship and coefficient of determination. The plot for the XY modulus and layer height similarly show a weaker relationship both for magnitude and coefficient of determination. Being as these results are less characteristic of the relationship than the initially performed analysis an ANOVA was not performed.

For the 45 degree infill samples the beads, presumed to be uniform in this analysis, will produce a consistent porosity due to the pattern throughout the gauge length. Effects of the bead profile changing between peaks and valleys of the previous layer's bead are presumed to be negligible for this analysis.

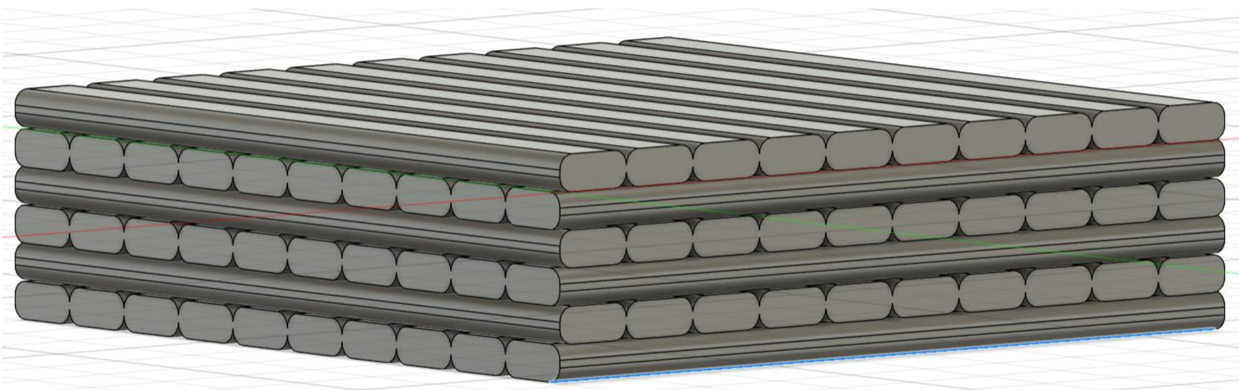

Figure 35: Fusion360 model depicting +-45 degree infill pattern.

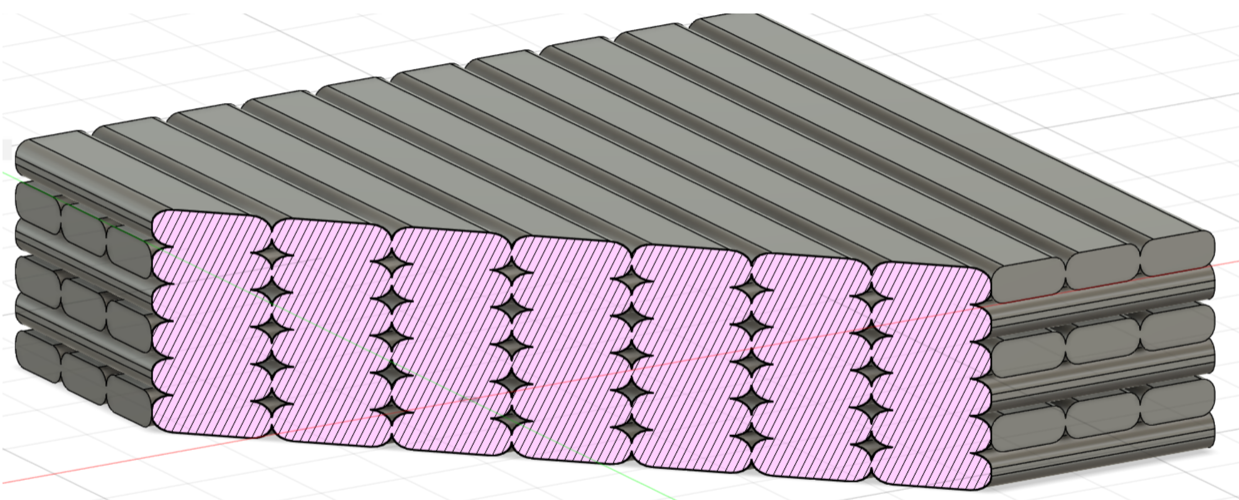

Figure 36: Fusion360 model depicting cross section taken perpendicular to load direction of +-45 degree samples.

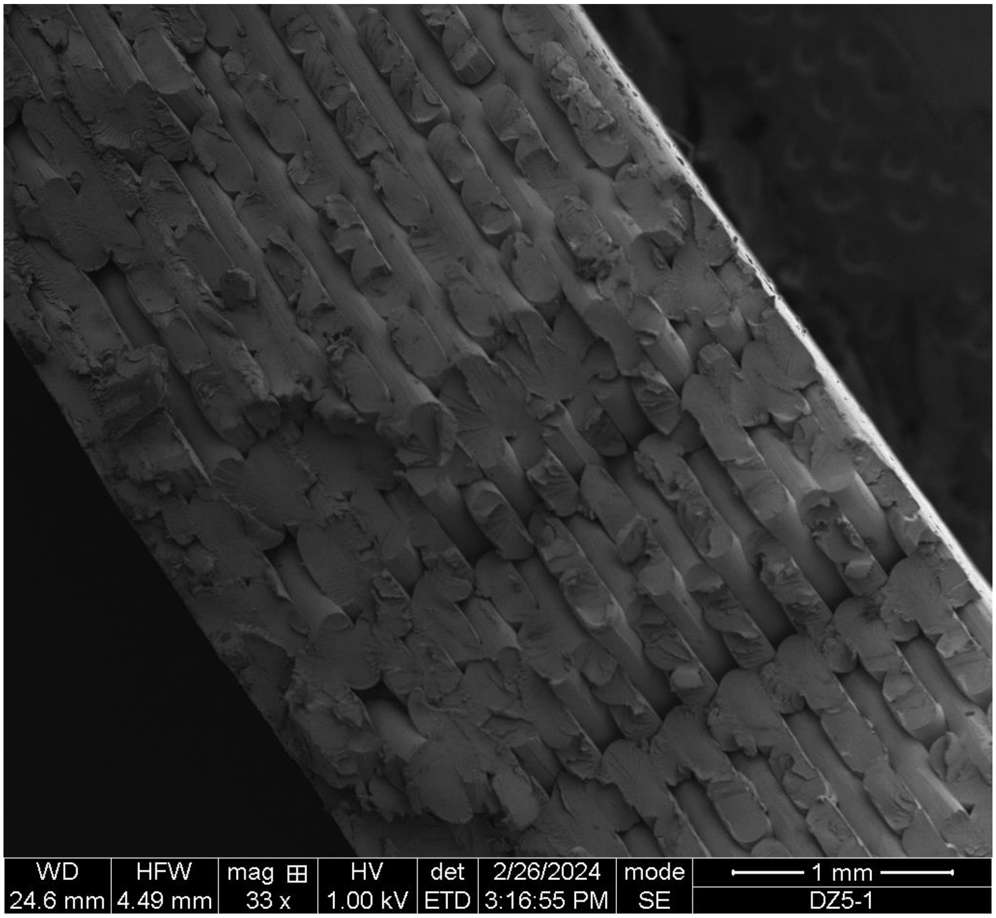

Figure 37: SEM image of break surface for sample #43, +-45 degree infill pattern

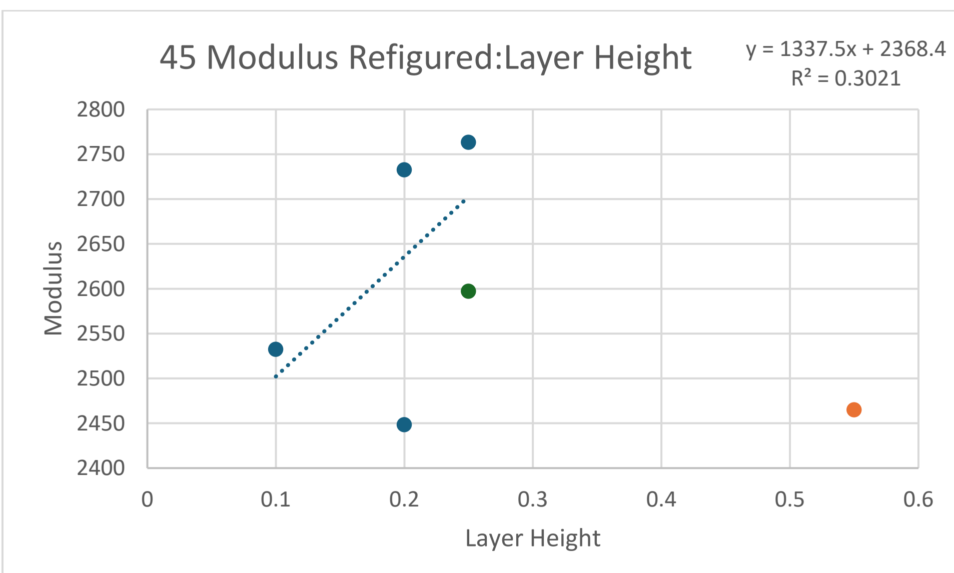

Figure 38: Plot of and Excel linear regression of modulus refigured for porosity by layer height for +- 45 degree infill sample sets with no observed flaws in the entire set.

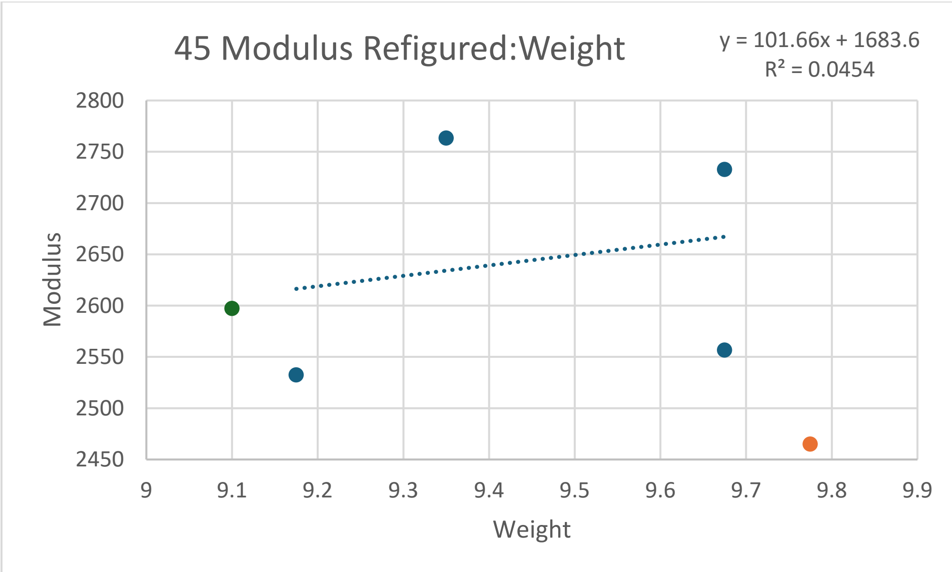

Figure 39: Plot of and Excel linear regression of modulus refigured for porosity by average sample weight for +- 45 degree infill sample sets with no observed flaws in the entire set.

The reexamination yielded a lower coefficient of determination and a lower magnitude of the relationship for the modulus and layer height. The modulus and weight relationship was shown to be lower and have a lower coefficient of determination than the initial analysis performed. Being as these results are less characteristic of the relationship than the initially performed analysis an ANOVA was not performed.

4.3 Reexamining Analysis with all unflawed samples included

The sets that included flawed samples frequently also contained samples where no flaw was noted. In this analysis the same analysis performed in section 4.1 is performed but with those samples included. This provides the opportunity to observe both how flaws present in a sample set cause deviation from expected parameter-property relationships and potentially increase confidence in suspected relationships from section 4.2.

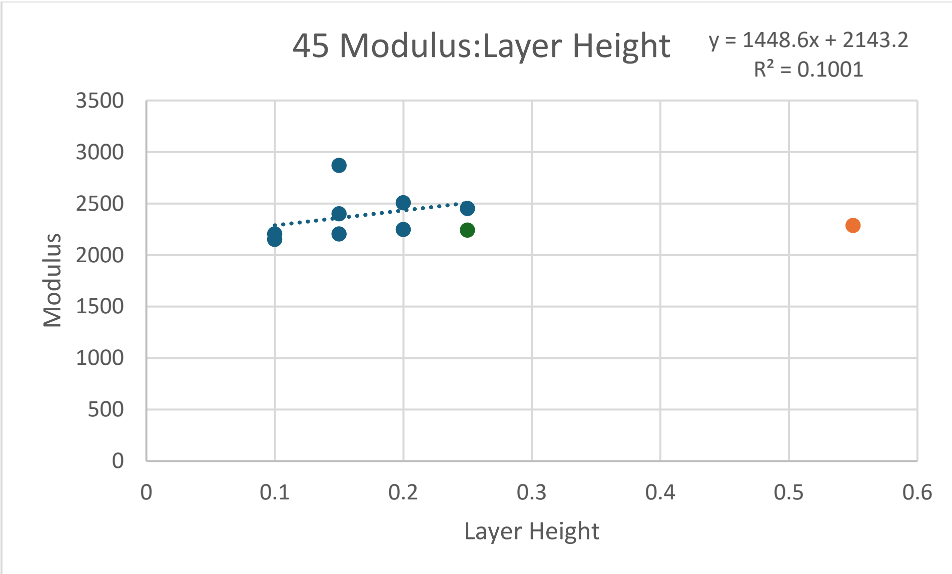

Figure 40: Plot of and Excel linear regression of modulus by layer height for +- 45 degree infill sample sets with no observed flaws in the samples.

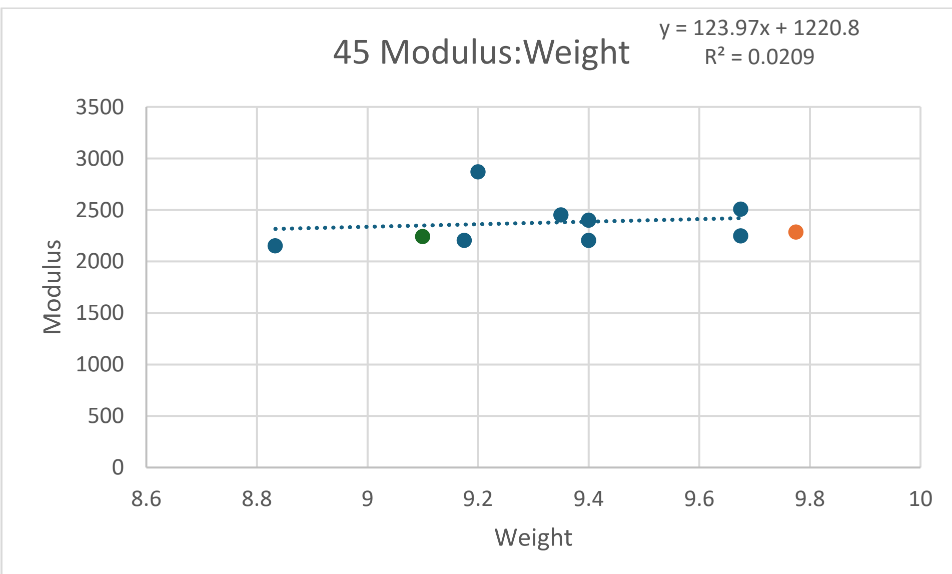

Figure 41: Plot of and Excel linear regression of modulus by sample weight for +- 45 degree infill sample sets with no observed flaws in the samples.

This analysis did not yield more significant results for the relationship between modulus in +-45 degree infill samples and layer height or sample weight. This analysis having a regression with a lower coefficient of determination would suggest that potentially unobserved flaws in the samples introduced negatively impacts the ability to estimate the modulus. This analysis did have two sample sets that were removed from consideration due to being suspected outliers.

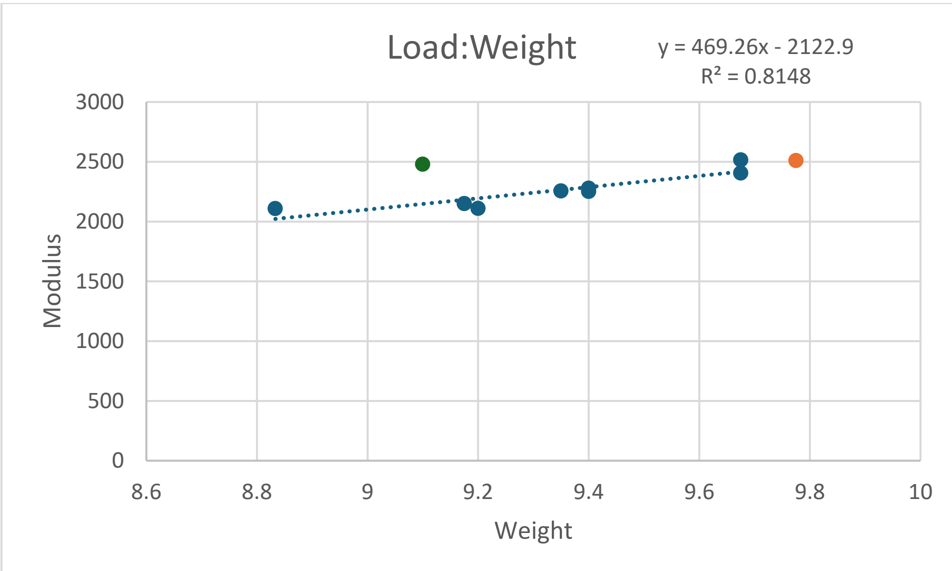

Figure 42: Plot of and Excel linear regression of load by sample weight for +- 45 degree infill sample sets with no observed flaws in the samples.

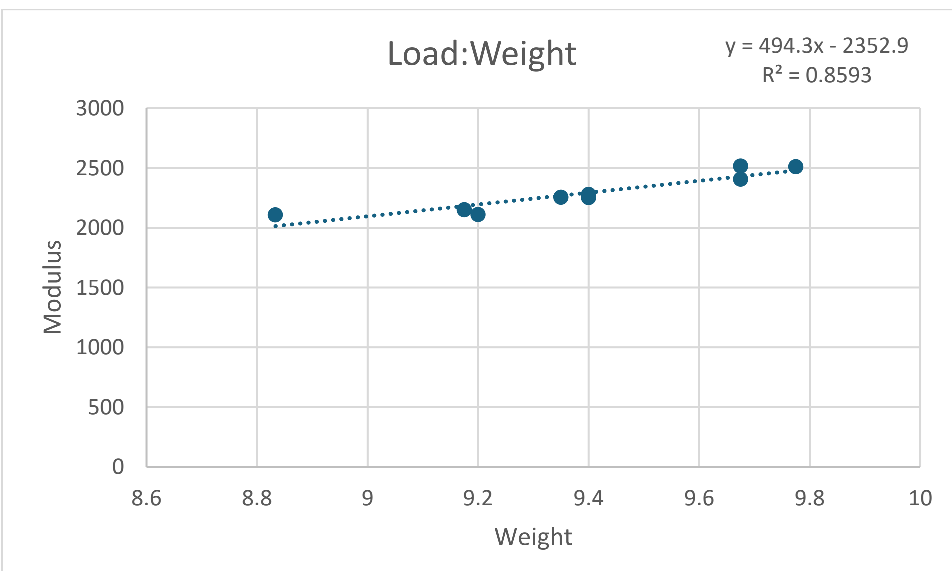

Figure 43: Plot of and Excel linear regression of load by sample weight for +- 45 degree infill sample sets with no observed flaws in the samples and 0.8mm nozzle sample included in data.

The load-weight relationship showed a lower coefficient of determination than the analysis performed without the samples introduced here, this coefficient being above .8 is still sufficiently high enough to suggest the load capacity follows this relationship and is further reinforced by including the 0.8mm data point as was done in section 4.2. The lower coefficient of determination here would suggest that potentially unobserved sample flaws can lower the ability to estimate this relationship although still sufficient to make estimations.

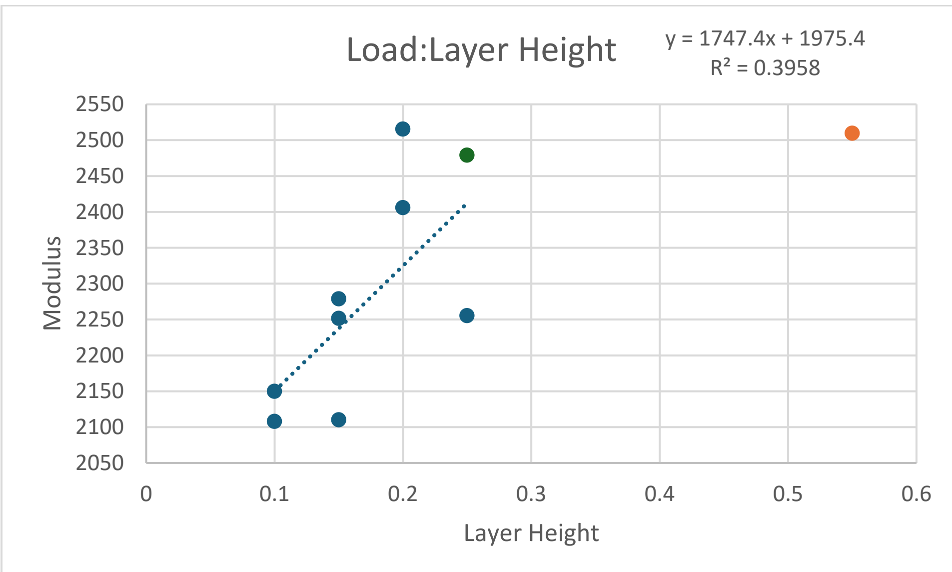

Figure 44: Plot of and Excel linear regression of load by layer height for +- 45 degree infill sample sets with no observed flaws in the samples.

The load-layer height relationship showed over twice the coefficient of determination shown in the analysis without the newly introduced samples. This result of a more relevant relationship after introducing more data of a lower quality would suggest that the relationship between these properties could be found with a larger sample set as the primary problem in the initial analysis is a lack of sample size.

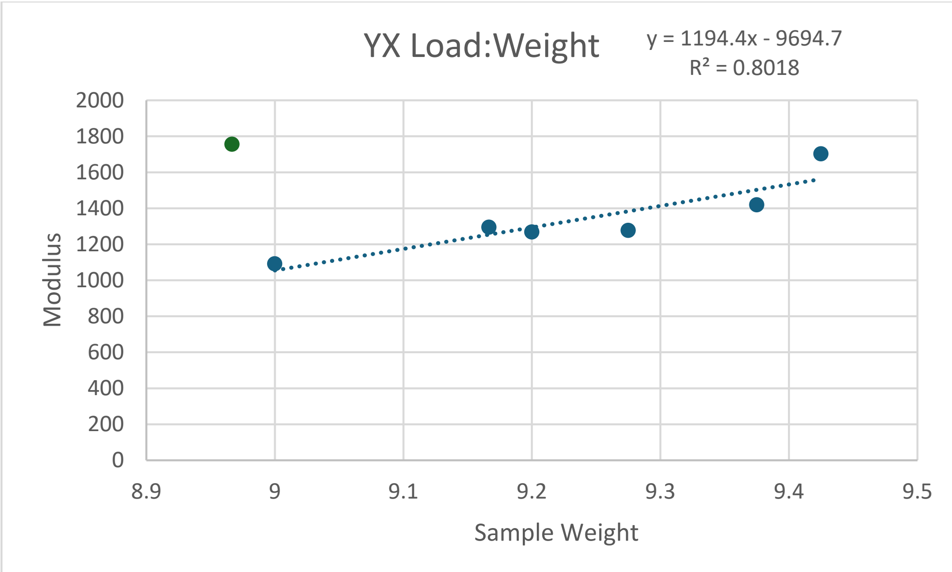

Figure 45: Plot of and Excel linear regression of load by weight for YX orientation infill sample sets with no observed flaws in the samples.

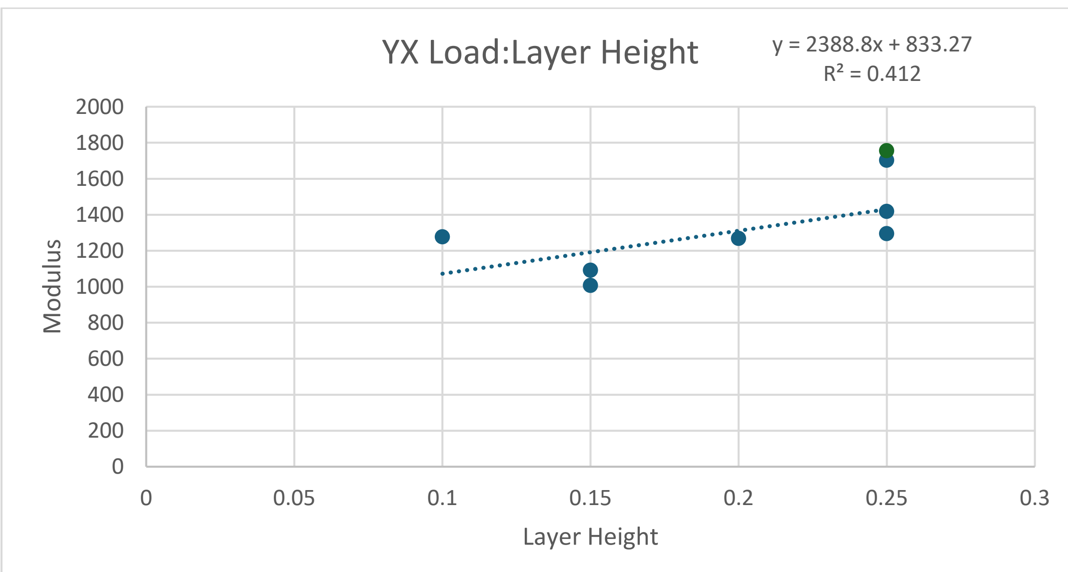

Figure 46: Plot of and Excel linear regression of load by layer height for YX orientation infill sample sets with no observed flaws in the samples.

The load-weight relationship for YX samples had an increase in coefficient of determination, after removing the same outlier from the analysis in section 4.2, suggesting that this relationship could also be confirmed with a larger sample size. The load-layer height relationship also increased in coefficient suggesting this relationship could be determined with a larger sample size although still too low to conclude that this regression models that relationship.

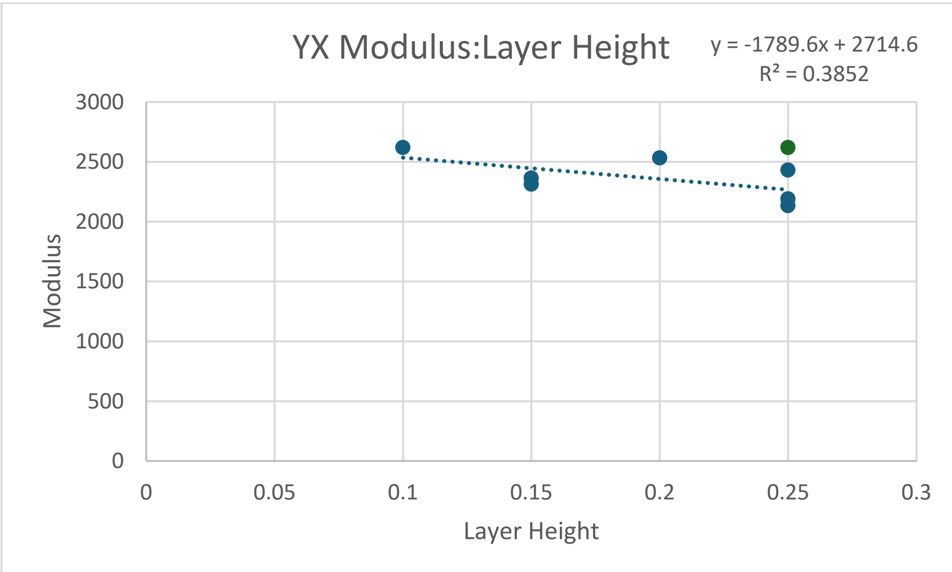

Figure 47: Plot of and Excel linear regression of modulus by layer height for YX orientation infill sample sets with no observed flaws in the samples.

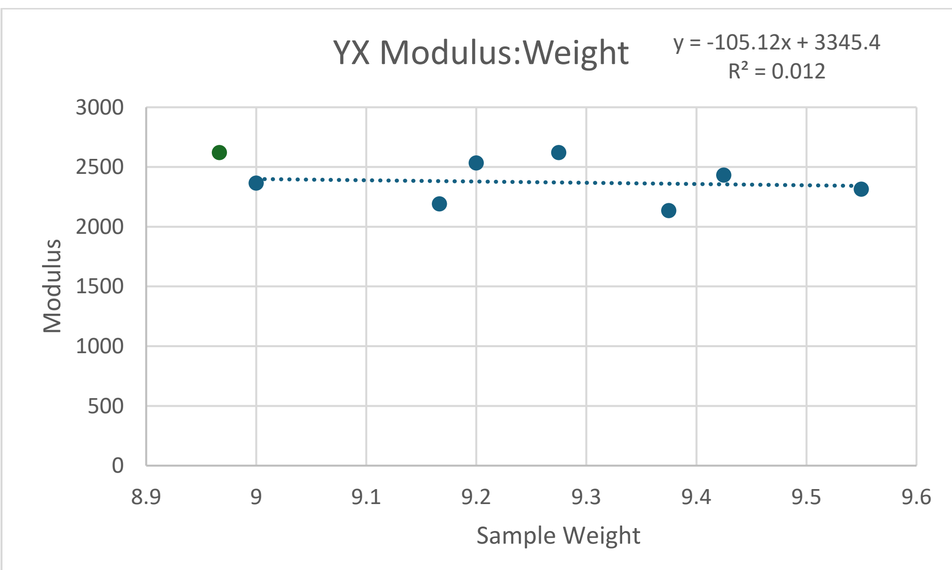

Figure 48: Plot of and Excel linear regression of modulus by sample weight for YX orientation infill sample sets with no observed flaws in the samples.

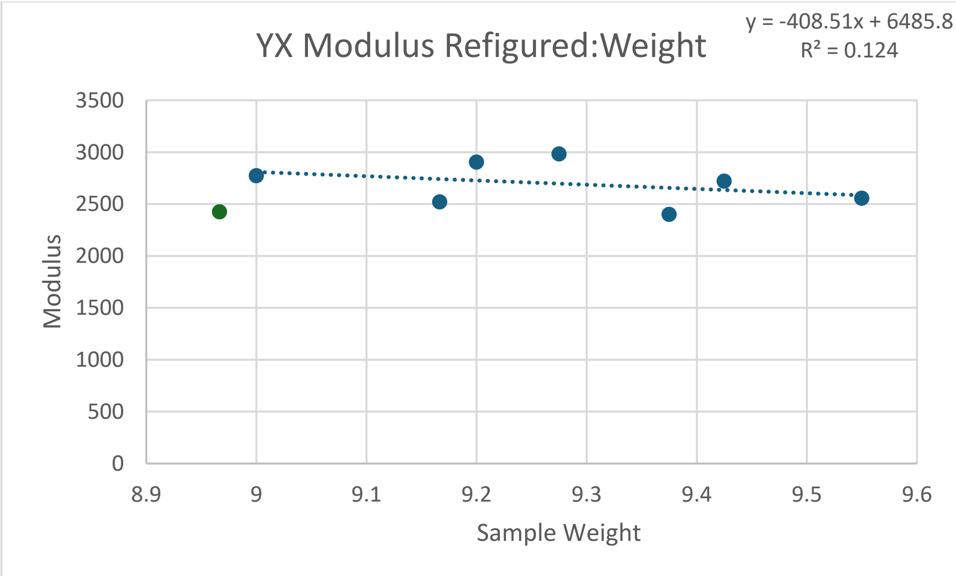

Figure 49: Plot of and Excel linear regression of refigured modulus by sample weight for YX orientation infill sample sets with no observed flaws in the samples.

The modulus-weight and modulus-layer height relationship again did not show high enough relevancy to determine a relationship exists here. The refigured modulus again showed a large increase in the modulus-weight relationship but is still a very low coefficient of determination. It is noted that there was only one additional sample set determined to be suitable for inclusion into the YX analysis.

A reexamination with all unflawed samples included for the XY orientation infill samples found all but one sample sets to be outliers. With an overwhelming portion of samples without observable flaws from sample sets that had a flaw observed being outliers it was determined this did not need to be included as it did not yield significant results for examination.

4.4 Reexamining Processes for Potential Uncaptured Variables

The decision to retain the perimeter printed on the samples is recognized as having the potential to introduce additional variables particularly in the form of the infill-perimeter overlap and the printer acceleration speeds for the bead path turnaround at the perimeter.

The processing parameters of the samples were kept very consistent with only adjustments to produce adequate print quality made, however the post-manufacturing parameters were not kept as tightly controlled. Particularly some samples cooled in the printer overnight while others were removed immediately after printing. The study by Kuzmina et, al.[11] did not show impact on mechanical properties from cooling conditions and room temperature of the facility the samples were removed in is tightly controlled however this variation between cooling in the printer and cooling in the room is noted as a possible source of uncaptured variables.

Sample filament was dried prior to sample manufacturing and stored in the machine's material storage however filament was not tested for moisture content prior to sample production. Samples were inspected for signs of moisture contamination with any such samples noted. Effects of moisture content below visually observable defects could be a source of pre-printing uncaptured variables.

Sample age at time of testing could also be analyzed, however it was noted in reviewed works that samples had been found to be very repeatable[16] between manufacture dates with later testing albeit with a much shorter overall timeframe between manufacture-testing and with a different production machine. The samples were stored at room temperature and kept out of sunlight, however a shorter timeframe could remove these from consideration entirely or further documentation could be made into another study. Samples were allowed 1-2 hours for temperatures to stabilize if stored in the author's vehicle which had become hot or cold during class before materials testing however this was not a thoroughly recorded scenario and recording this could also remove any effect from consideration.

Chapter 5: Conclusions and Future Work

5.1 Conclusions

The relationship between modulus and either layer height or sample weight for +- 45 degree infill sample sets was found to be likely although the relationship could not be determined at this time. The relationship for load and weight is believed to be determined with this study with a highly relevant regression to the data and an ANOVA indicating statistically significant sampling. The load and layer height was indicated to have a relationship by the ANOVA and a notably relevant regression however the regression was not relevant enough to confirm this regression as the relationship, increasing relevance from introducing lower quality data would indicate that this relationship could be determined with a larger sample size.

The relationship between modulus and either layer height or sample weight for YX orientation infill sample sets was found to be unlikely to exist in a statistically significant manner. The relationship between load and weight for YX samples was suggested to be present although the sample size was too small to confirm the regression as characterizing this relationship. The relationship between load and layer height was also suggested to exist but the regression did not have a high enough coefficient of determination to conclusively determine the relationship at this time. It is suggested from increasing relevance when including lower quality data that a larger sample size could confirm this relationship.

The XY modulus relationship to the layer height or the sample weight was suggested to exist although this study did not find a regression that could be evidenced as describing this relationship. Refiguring the modulus based on the porosity did not yield a more relevant relationship for the modulus. The load was found to not be significantly changed by the density or layer height.

5.2 New Hypothesis

The hypothesis for the relationships in +-45 degree infill patterns processing parameters is still believed to be the same with it estimated that the observed results are a measurable impact on both the load and the modulus when varying the weight of the samples. The bead in these samples both varied in fusion area between beads and the beads themselves carrying load along the bead. This gave us a change in stiffness as the beads will have a change in fusion area that experiences shear and a change in the porosity of the loaded cross section.

The hypothesis for the YX orientation infill pattern is similarly unchanged from the initial hypothesis with the changing bead geometries and densities not being found to significantly affect modulus but evidenced to affect the load bearing capacity of these samples.

The hypothesis for the XY infill orientation samples has changed significantly from the original hypothesis. It was originally assumed that the density would cause a large change in the load capacity of XY samples with no significant change in the modulus. The results suggest the opposite and that the load capacity is largely unchanged with a low change in the modulus. For these samples this would suggest the geometry changes cause a change in factors determining stiffness which was presumed to be minimal originally, factors assumed to affect stiffness were theorized as primarily inter-bead interactions. With the negative slopes of the regressions it would suggest that some aspect of processing this orientation actually lowers the stiffness of this orientation when increasing the layer height and density of the samples. This would go against inter-bead interactions being a dominate factor in stiffness for XY samples and would suggest another factor such as inter-bead stress formation during cooling or bead overall straightness changing in consistency throughout the bead alignment holds would produce a larger impact on perceived stiffness.

5.3 Future work

Expanding sample sets for the orientations found to be significantly influenced by the tested parameters would be a primary area to continue this research in the future, particularly as expanded sample sets focused on the areas where this thesis found results could be built upon for developing material property curves. These samples could also include sets with the perimeters machined off to match the samples performed by other manufactures.

The substantial portion of samples set aside for testing with the DIC setup is a very large dataset describing how stress flows through samples which match the samples analyzed in this thesis. An analysis of how the stress flows through these samples would be an area to continue this research both into the effects the studied variables have on how stress moves through the samples and as a study into how stress flows from the sample infill into the sample perimeters. If expanded sample sets described in the previous paragraph were performed it could serve as an opportunity to simultaneously produce samples for DIC testing which could be compared for a deeper analysis of the effects of the infill-perimeter settings on sample performance.

The flawed samples which were retained and tested serve as another area where future work could be performed. These samples provide a data set for analyzing print defects which could provide better understanding of the impact of printing defects on material properties. The flawed samples tested with DIC also have the possibility to yield additional insights into the stress mechanics of defective or damaged parts. Conversely insights into the material properties and stress mechanics of defective material could give insights into mitigations for material damage or acceptable bounds of material defects.

References

1. Stratasys, *Certified Additive Manufacturing for Aircraft Interiors*. Library of Congress: https://cdn.loc.gov/copyright/1201/2018/exhibits-043018/class12/Ex.%2012-A%20(Stratasys).pdf.
2. Stratasys, *ULTEM™ 9085 Resin TDS*. 2021: https://www.stratasys.com/siteassets/materials/materials-catalog/fdm-materials/ultem-9085/mds_fdm_ultem9085_0921a.pdf.
3. Swanson et al, P.W.T., Paul J. Leavitt, Peter J. Karwoski, Joseph E. LaBossiere, and Robert L. Skubic, *HIGH TEMPERATURE MODELING APPARATUS*, in *US Patent Office*, U.P. Office, Editor. 2004, Stratasys, Inc.,: United States.
4. L.G. Blok, M.L.L., H. Yu, B.K.S. Woods, *An investigation into 3D printing of fibre reinforced thermoplastic composites.* Additive Manufacturing, 2018. **22**: p. 11.
5. Inc., D.S., *Industrial scale, large format*

additive manufacturing solutions. 2023: https://www.3dsystems.com/sites/default/files/2024-01/3d-systems-titan-printer-brochure-usen-2023-12-1_a4-web.pdf.
6. Inc., M., *PRODUCT SPECIFICATIONS FX20*. 2024: https://s3.us-east-1.amazonaws.com/static.markforged.com/downloads/F-PR-3016-2.pdf.
7. Inc., S., *FDM Nylon 12CF MDS*. 2025: https://www.stratasys.com/siteassets/materials/materials-catalog/fdm-materials/nylon-12cf/mds_fdm_nylon-12cf_0325a.pdf?v=493d90.
8. Tools, I.M., *MASTERPRINT® 3X THE LARGEST EXISTING THERMOPLASTIC 3D PRINTER*. 2021: https://www.multistation.com/voy_content/uploads/sites/4/2019/03/masterprint-3x.pdf.
9. Tools, I.M., *MASTERPRINT® 5X 5 AXES LARGE FORMAT INDUSTRIAL THERMOPLASTIC 3D-PRINTER*. 2021: https://exhibitorsearch.messefrankfurt.com/images/original/mics/10000133202201/0012214280/1668005164352_1444672248.pdf.
10. Inc., S., *Antero 800NA Annealed*. 2018: https://stratasysstorage01.file.core.windows.net/portal10-files-prod/b8637e94-510a-4071-b002-7cf99dbc5967/Antero%20800NA%20Annealed%20-%20EN%20FDM%20Material%20Data%20Sheet.pdf?sv=2019-07-07&sr=f&sig=90q2Dy7hk%2BgSzhOnUUHAknRf46EFypk6Vzfx243Fp4I%3D&st=2025-03-18T04%3A55%3A06Z&se=2025-03-19T10%3A55%3A06Z&sp=r&rsct=application%2Fpdf&rsce=UTF-8&rscd=inline%3B%20filename%3D%22Antero%20800NA%20Annealed%20-%20EN%20FDM%20Material%20Data%20Sheet.pdf%22.
11. Tatjana Glaskova-Kuzmina, D.D., J¯anis J¯atnieks, Partel-Peeter Kruuv, Aleksejs Zolotarjovs, Ernests Einbergs, and Edgars Vanags, *Effect of Printing Direction and Post-Printing Conditions on*

Bending Properties of ULTEM 9085. Journal of Composites Science, 2023. **7**.
12. R.J. Zaldivar, D.B.W., T. McLouth, D.N. Patel, K. Schmitt, J.P. Nokes, *Influence of processing and orientation print effects on the mechanical and thermal behavior of 3D-Printed ULTEM® 9085 Material.* Additive Manufacturing, 2017. **13**: p. 71-80.
13. Agnes Bagsik, V.S., *Mechanical properties of fused deposition modeling parts manufactured with ULTEM 9085.* ANTEC, 2011: p. 1294-1298.
14. Elisa Padovano, M.G., Paolo Concialdi, Gianni Lucco, and Claudio Badini, *Mechanical and Thermal Behavior of Ultem® 9085 Fabricated by Fused-Deposition Modeling.* Applied Sciences, 2020. **10**.

15. R.J. Zaldivar, T.D.M., G.L. Ferrelli, D.N. Patel, A.R. Hopkins, D. Witkin, *Effect of initial filament moisture content on the microstructure and mechanical performance of ULTEM® 9085 3D printed parts.* Additive Manufacturing, 2018. **24**: p. 457-466.
16. Rachael Wratkowski, E.O.H., Bruce Solheim, Chris Cates, Chris Rollag, Sanja Wallace, Adam R. Pawloski, *A Characterization of the Repeatability and Performance of Stratasys Fused Deposition Modeling (FDM) Systems*. 2022, Stratasys Inc.: https://www.stratasys.com/contentassets/1081bb4d532b4d38a9e1fed9ba4d8c13/repeatability-and-preformance-of-stratasys-fused-deposition-modeling-fdm-technology.pdf?v=4a6fdd.
17. Moon, Y.Z.a.S.K., *The Effect of Annealing on Additive Manufactured ULTEM™ 9085 Mechanical Properties.* materials, 2021. **14**.
18. Yifan LV, D.D., Stepan KOBENKO, Sarat SINGAMNENI, Tatjana GLASKOVA-KUZMINA3, *Evaluation of the Fire-retardancy of ULTEM 9085 Polymer Composites Processed by Fused Deposition Modelling.* Materials Science, 2022. **28**.
19. Inc., S., *Maintaining FDM Material Properties Through Proper Drying and Storage*. 2021, Stratays Inc. : https://support.stratasys.com/download/D8AE0686-7064-42A6-B8F9-A9B60F294CE1#:~:text=1.,of%2030%20minutes%20before%20printing.
20. Inc., E., *Essentium 9085 technical data sheet*. 2020: https://nexa3d.com/wp-content/uploads/2024/08/TDS-Essentium-9085.pdf.
21. 3DXTECH, *Technical Data Sheet: ThermaX™ PEI [Made using ULTEM™ 9085]*. https://cdn.shopify.com/s/files/1/0625/4185/6821/files/THERMAX_PEI_9085_TDS_v4.pdf?v=1723942766.
22. Inc., M., *ULTEM™ 9085 Filament and*

Carbon Fiber for ULTEM™

Filament. 2023:
https://s3.amazonaws.com/mf.product.doc.images/Datasheets/Material+Datasheets/ULTEM%E2%84%A2_9085_Filament_Material_Datasheet.pdf.
23. Inc., S., *ULTEM FILAMENT AM9085F*. 2020: https://store.3dgence.com/data/links/8cbdd13bf2c3eee632d08a15d71d09ea/191_794.pdf.
24. Inc., S., *PROCESS SPECIFICATION, ANTERO 840CN03*. https://www.msudenver.edu/wp-content/uploads/2022/03/Antero_Process-Specification_840CN03_3.28.2022.pdf.
25. ASTM, *Standard Test Method for Tensile Properties of Plastics*. 2015.
26. ASTM, *D 618 - 00*, in *Standard Practice for Conditioning Plastics for Testing*. 2000, ASTM.
27. Sabic, *ULTEM Resin 9085 Global Technical Data Sheet*. 2024, Sabic: https://materialfinder.sabic-specialties.com/material/ultem-resin-9085.